UNIVERSITY OF GENOA

PHD PROGRAM IN CLINICAL AND EXPERIMENTAL IMMUNOLOGY

Bone Marrow-Derived Extracellular Vesicles Carry RNAs Shaping The Tumor Microenvironment in High-Risk Neuroblastoma Patients

Martina Morini

Thesis submitted for the degree of Doctor of Philosophy (38° cycle)

Prof. Roberta Castriconi — Advisor
Prof. Cristina Bottino — Advisor
Prof. Simona Sivori — Head of the PhD Program

Summary

1. Abstract

Background

Despite the intensive treatment, the survival rate of high-risk neuroblastoma (HR-NB) patients remains low. Over 10% of patients have tumors that lack the expression of GD2, a NB-associated ganglioside, making them ineligible for anti-GD2 antibody immunotherapy. Therefore, the development of novel therapeutic strategies to enhance immunotherapy efficacy and mitigate side effects is urgently needed. Circulating small extracellular vesicles (sEVs) can contribute to tumor progression by promoting metastasis, immunosuppression, and resistance to treatment, ultimately interfering with antibody-dependent cellular cytotoxicity.

Aims

We aimed at profiling the RNA content of bone marrow (BM)-derived circulating sEVs to investigate their ability to shape the tumor microenvironment (TME), identifying new therapeutic targets to improve immunotherapy outcomes.

Methods

We isolated sEVs from BM plasma samples of HR-NB patients at diagnosis with or without BM infiltration (n=27). We assessed quality and quantity of isolated EVs and performed total RNA sequencing.

Results

We implemented a novel protocol for the efficient isolation of sEVs from 0.5 ml of plasma derived from BM. The average quantity of RNA obtained ranged from 300 to 600 ng. We observed that sEVs carry the transcripts of genes (mRNAs) microRNAs (miRNAs) and long non-coding RNAs (lncRNAs) involved in cell metabolism, cell signaling and immune response, such as Natural Killer-cell mediated cytotoxicity and chemokine signaling. sEV-miRNAs and lncRNAs showed differential expression between infiltrated and non-infiltrated BM samples. Three sEV-miRNA downregulated in infiltrated BM samples were involved in the regulation of PD1/PDL1 interaction and signaling. Moreover, bioinformatic integration analysis of mRNAs, lncRNAs and miRNAs stratified HR-NB patients into three clusters, identifying a signature associated with the hypoxic status and the poor prognosis. These results suggest that BM-derived sEVs carry RNAs contributing to an immunosuppressive TME, negatively affecting treatment response and clinical outcome.

Conclusions

BM-derived sEVs carry RNA molecules that regulate immune pathways, hindering the response of HR-NB patient to immunotherapy. These findings provide insights into the role of sEVs in TME modulation and identify potential targets for improving immunotherapy.

2. Introduction

2.1. Neuroblastoma

Neuroblastoma (NB) is a pediatric cancer of the sympathetic nervous system originating from neural crest-derived cells. NB is the most frequent extra-cranial solid tumor in children younger than 5 years with an age-adjusted incidence rate of 8.3 cases per million persons[1]. In particular, the peak of incidence is observed at 18 months of age, while the incidence significantly decreases to less than 5% after the age of 10 years (one per 10 million persons)[2]. Neuroblastoma patients can present with systemic symptoms, such as fever or weight loss, but the symptomatology is mainly dependent on the localization of the primary tumor and, eventually, of metastases[3].

2.1.1 Neuroblastoma origin

The neural crest is an embryonic structure originating from the closing of the neural tube. Neural crest cells (NCCs) are multipotent stem cells able to migrate to different body sites, differentiating towards different cell types, including sympathetic neurons of the peripheral nervous system and the adrenal medulla, which represents the primary NB site. According to this embryonic origin, NB cells secrete the sympathetic catecholamines epinephrine and norepinephrine[4,5].

NCCs differentiation is regulated by several pathways, including BMP (Bone Morphogenetic Protein), WNT, Notch, and FGF (Fibroblast Growth Factor) signaling pathways, that trigger the expression of transcription factors activating the epithelial to mesenchymal transition, conferring NCCs migratory properties. When this signaling is altered, together with complex combination of multiple genetic or epigenetic factors, neuroblasts can arise and eventually NB tumor develops[5,6].

Among the key factors involved in neuroblast differentiation and maturation to sympathetic neurons we can find the transcription factor PHOX2B (Paired-like homeobox 2b) that works in conjunction whit ASCL1 (Achaete-scute family bHLH transcription factor 1), also known as Mash1 (Mammalian achaete scute homolog-1), and GATA2 and GATA3 (GATA-binding protein 2 or 3) genes. Additional relevant players in NB development are TH (Tyrosine Hydroxylase), which is the first enzyme involved in the synthesis of catecholamines, DBH (Dopamine Beta-Hydroxylase), ISL1 (ISL LIM homeobox 1), NTRK1 (Neurotrophic Receptor Tyrosine Kinase 1)[7].

A hallmark of NB is its heterogeneity, which often makes the stratification patients difficult. The accurate classification of patients into risk groups, based on clinical and biological markers, is mandatory for the selection of the best therapeutic option at an early stage of the disease.

2.1.2. Neuroblastoma staging system and treatment

The first International Neuroblastoma Staging System (INSS), which is based on the extent of surgical resection and the presence/absence of metastases, was introduced in 1988.

The INSS staging system subdivides neuroblastoma patients into six different groups:

Group 1: Localized tumor, grossly resected, no lymph node involvement;

Group 2A: Unilateral tumor, incomplete gross excision, negative lymph nodes;

Group 2B: Unilateral tumor with positive ipsilateral lymph nodes;

Group 3: Tumor infiltrating across midline or unilateral tumor with contralateral lymph nodes or midline tumor with bilateral lymph nodes;

Group 4: Distant metastatic disease;

Group 4S: Localized primary tumor as defined by stage 1 or 2 in patients under 12 months with dissemination limited to the liver, skin, and/or bone marrow (<10% involvement)[8].

The staging system was revised to harmonize the criteria used with new information from neuroblastoma genetics; thus, the International Neuroblastoma Risk Group Staging System (INRGSS) was introduced in 2009. This classification system is based on Imagine-defined risk factors (IDRFs), defined as pre-operative radiological features observed in imaging studies without considering surgical resection.

The INRG staging system defines four groups:

Group L1: Localized tumor with no image-defined risk factors;

Group L2: Localized tumor with one or more image-defined risk factors;

Group M: Distant metastatic disease;

Group MS: Metastatic disease in children under 18 months with metastases limited to skin, liver, and/or bone marrow (<10% involvement)[9].

The INRGSS was subsequently incorporated into a new protocol developed by the Children's Oncology Group, leading to the INRG risk classification system (Table 1). It is based on different criteria: age at diagnosis, with a specific cut-off fixed between 12 and 18 months, disease stage based on the INRGSS staging system, tumor histology, MYCN status, tumor cell ploidy (diploid vs. aneuploid), and chromosomal aberrations[9].

Importantly, the amplification of the MYCN gene was the first clinically relevant genetic biomarker in NB. MYCN status can be determined by fluorescence in situ hybridization, and samples with a 4-fold increase in signal are considered amplified[10].

According to INRG staging system, patients are classified into four groups: very low/low (LR), intermediate (IR), and high risk (HR).

LR patients have survival rates >95% and constitute about 30% of all NB patients. They mostly present localized disease amenable to surgical resection due to the absence of Image-defined risk factors (IDRF) and without MYCN amplification. Most LR patients do not require chemotherapy unless there are organ or life-threatening symptoms. Many LR patients undergo partial or complete surgical resection, and in some cases, even spontaneous regression has been observed.

Approximately 20% of the NB patients fall into the IR group with an overall survival (OS) of about 90%. In most studies, IR patients receive from 2 to 8 cycles of chemotherapy and usually undergo surgical resection.

About 50% of patients have HR disease. According to INRG classification, stage M patients with age at diagnosis over 18 months or diagnosed with NB before 18 months but with MYCN amplification are classified as HR. Amplified MYCN is one of the strongest predictors of HR disease; indeed, patients with stage L1, L2 or MS with MYCN amplification still fall into the HR group. Metastases are observed in the bone marrow, in bone and regional lymph nodes, while involvement of the central nervous system and lungs is rare[11]. Bone marrow is a site of metastasis in 80% of HR-NB patients and represents the most common site of resistance to therapy and NB relapse[11].

Table 1. International Neuroblastoma Risk Group (INRG) classification system

INRG Stage	Age months	Histological Category Grade of Tumor Differentiation	MYCN	11q Aberration	Ploidy	Risk Group
L1/L2		GN maturing GNB intermixed				Very Low
L1		Any, except GN maturing or GNB intermixed	NA			Very Low
			Amp			High
L2	<18m	Any, except GN maturing or GNB intermixed	NA	No		Low
				Yes		Intermediate
	≥ 18m	GNB nodular, differentiating NB	NA	No		Low
				Yes		Intermediate
		GNB nodular, poorly differentiated or undifferentiated NB, poorly differentiated or undifferentiated	NA			Intermediate
			Amp			High
M	<18m		NA		Hyperdiploid	Low
	<12m		NA		Diploid	Intermediate
	12m-18m		NA		Diploid	Intermediate
	<18m		Amp			High
	≥18m					High
MS	<18m		NA	No		Very Low
				Yes		High
			Amp			High

Table 1: INRG classification system from 'The International Neuroblastoma Risk Group (INRG) Classification System: An INRG Task Force Report' published by American Society of Clinical Oncology, 2009. GN = Ganglioneuroma, GNB = Ganglioneuroblastoma, NB = neuroblastoma, NA = MYCN not amplified, Amp = MYCN amplified.

Significant progress has been made in the treatment of HR patients. The 5-year overall survival has improved significantly over the last 20 years, from 29% in patients diagnosed from 1990 to 1994 to 50% in patients diagnosed from 2005 to 2010. However, further improvement of patient survival is needed, especially for patients with refractory or relapsed neuroblastoma, who can rarely be cured.

The current standard treatment for HR neuroblastoma includes three phases: induction chemotherapy, consolidation, and maintenance.

Treatment starts with multiple cycles of induction chemotherapy with platinum-based drugs, anthracyclines, and alkylating agents. The main purpose of this step is to reduce the tumor burden, making it more amenable to surgical resection. The induction phase also includes surgery and apheresis to harvest patient's hematopoietic stem cells (HSCs). Surgery is performed towards the end of induction chemotherapy to remove the remaining primary tumor. Complete surgical resection is not always possible or safe, as the primary tumor often grows near important blood vessels or invades neural foramina.

After surgery, consolidation myeloablative therapy is applied, which consists of high-dose chemotherapy and radiation treatment on the primary tumor bed. This therapy is followed by transplantation of autologous stem cells retrieved during the induction phase.

Maintenance therapy includes combined treatment with retinoid drugs and immunotherapy and can include the administration of cytokines such as GM-CSF and interleukin-2, which, however, has shown poor benefits and important side effects. The retinoid used is 13-cis-retinoic acid (isotretinoin), which acts by promoting the differentiation of tumor cells towards a mature phenotype. Immunotherapy uses chimeric antibodies that target GD2, a disialoganglioside expressed in neuroectodermal tumors, including NB.

Current research is focusing on further intensification of therapy to improve the prognosis of HR-NB patients. Liquid biopsy analysis is a strategy emerging as an important aid in the study and diagnosis of HR-NB patients[3].

2.2. Liquid biopsies and their clinical significance

Liquid biopsy refers to analyte analyses in performed on body fluids such as blood (the most investigated and easily accessible source), urine, saliva, bone marrow, or cerebrospinal fluid. Standard needle biopsies often result in inadequate material for downstream molecular analysis, thus studying alternative sources of biological material could provide insight into tumor features.

Non-invasive sampling is one of the main advantages of most liquid biopsies compared to tissue biopsies; they avoid surgical intervention, except for bone marrow analysis, which, however, is highly

informative. The simultaneous evaluation of different biomarkers allows a real-time monitoring of the disease, capturing disease evolution and patients' responses to treatment.

Being a novel approach, the main challenge for the use of liquid biopsies is the possibility of referring to standardized protocols. For this reason, variability in sample collection, processing, and methods of analysis can affect the reproducibility and reliability of the results. Moreover, the analyses generate complex datasets of results, making the clinical interpretation challenging.

Liquid biopsies, however, play an important role in oncology since tumor-derived components such as cells, DNA, and small extracellular vesicles are released within biological fluids.

While the primary tumor mass grows, some cells can detach and enter in blood and lymphatic vessels, through which they can reach new body sites and initiate metastases. These cells, defined as circulating tumor cells, maintain most of the characteristics of the mass from which they detach, and can be very useful to study tumor phenotype and heterogeneity[12].

Tumor cells can undergo apoptosis or necrosis, especially when tumor mass becomes large and poorly vascularized, releasing the so-called circulating tumor DNA (ctDNA). ctDNA carries tumor-specific mutations and alterations and can be an important source of biomarkers[13].

Tumor cells, as well as normal cells, secrete extracellular vesicles, structures composed by a phospholipid bilayer and containing several molecules like lipids, proteins, and nucleic acids. Extracellular vesicles are released in body fluids and are defined as the "bioprint" of the cell of origin, thus representing an important source to study tumor features[14].

The principles mentioned above makes liquid biopsies a powerful diagnostic tool with several potential clinical applications. Liquid biopsies help an accurate diagnosis by improving the genetic and molecular tumor profiling and by tracking changes in tumor-derived components, enabling the real-time assessment of disease progression[15].

In addition, liquid biopsies could provide insight into therapies' sensitivity or resistance by detecting mutations in circulating DNA. This analysis makes it possible to assess the risk of post-treatment metastasis or recurrence: the presence of circulating tumor cells or specific biomarkers indicates the persistence of the disease (minimal residual disease, MRD) or an increased risk of tumor relapse after the end of treatment[14]. In HR-NB patients, typical markers of MRD are PHOX2B or TH, usually detected in peripheral blood or bone marrow[16].

The analysis of many potential biomarkers contributes to the development of personalized treatment plans by enabling the selection of the best therapeutic options that selectively target mutated protein or relevant cellular pathways (personalized medicine). This approach aims to improve the clinical outcome by adopting more effective and long-lasting therapeutic solutions with limited side effects compared to current standard treatments[17].

Studies on the potential of liquid biopsies in neuroblastoma have increased in the past years, focusing mainly on ctDNA and extracellular vesicles.

2.3. Extracellular Vesicles

2.3.1. Biogenesis

Extracellular vesicles (EVs) are nano-sized particles released by different cell types for intercellular communication: they carry proteins, lipids, RNAs, and other biomolecules that can modulate the biological processes of the recipient cells. The phospholipid bilayer of EVs ensures stability to their molecular content. EV cargo is not randomly loaded, but it is determined by an active mechanism strictly dependent on the cell type of origin and its physiological or pathological state. Indeed, under pathological conditions, cells can increase EVs secretion, making them a valuable source of biomarkers for disease progression. Besides their cargo, which can be transferred to other cells, EVs have specific surface markers such as CD9, CD81, and CD63, which belong to the tetraspanin family[18].

In physiological conditions, EVs are released by all cell types and regulate several biological functions aimed at maintaining the tissues' homeostasis. For example, red blood cells release EVs to regulate clotting and immune response, immune cells, like lymphocytes and dendritic cells, release vesicles to prime and modulate the immune response, and endothelial cells release EVs to influence inflammation and vascular health[19]. EVs released from mesenchymal stem cells have mainly two therapeutic effects: tissue regeneration and immunomodulation. EVs released from stem cells can promote healing or repair of damaged tissues or reduce inflammation at the damaged site by downregulating the immune response[20].

Recipient cells can uptake EVs through different mechanisms: (i) membrane fusion between EVs and target cells, (ii) endocytosis from recipient cells followed by lysosome digestion to release EVs cargo, (iii) specific receptor-ligand recognition between ligands expressed on EVs surface and receptors exposed on target cells, (iv) release of EVs cargo in the extracellular space within the extracellular matrix which directly deliver molecules to the surrounding cells. Moreover, additional mechanisms have been proposed such as micropinocytosis or phagocytosis[21] (Figure 1).

The mechanism of EVs biogenesis and the EVs size help to classify these particles into two distinct categories: ectosomes and small extracellular vesicles (Figure 1).

Ectosomes are vesicles that arise directly from the outward budding of the cellular plasma membrane and comprise particles between 50 nm and 1 μm in diameter. The budding process is driven by alteration of calcium concentration: the plasma membrane loses contact with the cytoskeleton,

calcium-dependent enzymes alter the phospholipid asymmetry of the membrane to induce cytoskeleton contraction, leading to the cleavage of the budding vesicle from the plasma membrane[21]. Small extracellular vesicles (sEVs) have a diameter size ranging from 40 to 160 nm and an endosomal origin, which determines the presence inside the cargo of specific molecules such as ALIX, TSG101, syntenin-1, and syndecan. Biogenesis of sEVs starts with the formation of an early endosome through inward budding of the plasma membrane. Early endosomes mature to form the late endosome characterized by the intraluminal presence of multivesicular bodies (MBV). Late endosomes can fuse with lysosomes for degradation or with the plasma membrane to release their intraluminal vesicles (ILVs) into the extracellular space. Once released, ILVs are referred to as sEVs[22].

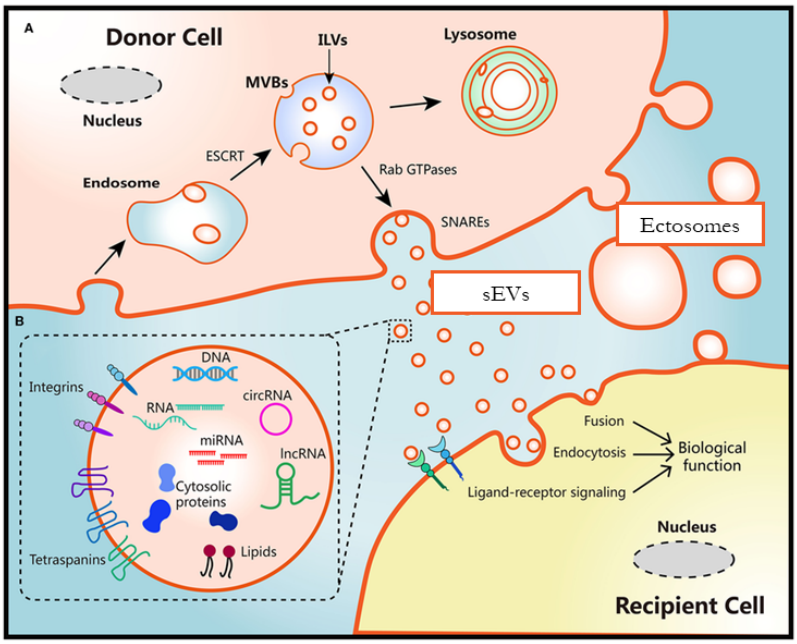

Figure 1: Biogenesis, cargo content, secretion, and uptake of sEVs or ectosomes (modified Quin Z. et al 2020)[23].

2.3.2. EVs derived from peripheral blood of NB patients

The EVs released by tumor cells reflect the cell of origin in terms of both their cargo and surface markers: NB-derived EVs express on their surface GD2, the marker typical of neuroectoderm-derived tumors, including most NB.

Tumor released vesicles promote tumor growth, thus the EVs' cargo may exert specific pro-tumor activities, modulating processes such as inflammation and complement activation, immune response, cell proliferation and apoptosis, and interaction with the ECM.

Our first study on EVs investigated blood-derived EV-miRNA profile in HR-NB patients before and after induction chemotherapy, aiming at identifying markers of treatment response. We identified a signature of three miRNAs, miR-342-3p, miR-29c, and let-7b, which were significantly

downregulated in patients with a poor response. These 3 miRNAs are involved in tumor suppression and chemoresistance acquisition; thus, their downregulation could lead to a poor response to induction chemotherapy in NB patients[24]. The same study revealed that the EV-miRNA profile can be used to determine a chemoresistance index for each patient towards each drug administered in the induction chemotherapy regimen, providing a molecular-based definition of response to treatment that could potentially redirect the therapeutic strategy[24].

Additionally, we demonstrated that EVs derived from peripheral blood of NB patients contain proteins that are upregulated or downregulated compared to control samples. The upregulated proteins include Neural Cell Adhesion Molecule (NCAM), an adhesion molecule known to be highly expressed in NB tumors, and Nucleolin (NCL), which has already been associated with NB patient poor prognosis. The downregulated proteins include Lumican and Decorin, proteoglycans that hinder cell migration, and VASP, a phosphoprotein regulating cell adhesion. These proteins were shown to have a diagnostic value, helping to identify NB patients. Moreover, high-risk and low-risk NB patients are characterized by different EV protein content. HR-NB sEVs showed high expression of Myosin 9, a factor stimulating macrophage migration and metastases formation, and of Fibronectin-1 and LTBP1, extracellular matrix components promoting cell migration and epithelial to mesenchymal transition. On the other hand, HR-NB EVs contain lower levels of calreticulin, a pro-phagocytic protein activating the immune response, and AKAP-12, a kinase inhibiting angiogenesis and cell migration. These proteins showed a high prognostic power in discriminating patients with high-risk and low-risk disease[25].

Circulating EVs from peripheral blood of NB patients were shown to have diagnostic and prognostic values, allowing a non-invasive monitoring of the disease. However, little is known about EVs released within the BM, the major metastatic niche of HR-NB patients.

2.3.3. EVs and their role in the tumor microenvironment

The tumor tissue is a complex system made of tumor cells and a set of different cell types essential for tumor growth, which constitute the tumor microenvironment (TME). These cells are recruited by the tumor cells themselves during the different stages of tumorigenesis, thus the TME is a dynamic system that follows the evolution of the tumor.

Cancer cells and cancer stem cells initiate the disease and drive tumor progression as they accumulate specific mutations that allow them to grow uncontrollably by exploiting various mechanisms.

The stromal compartment of the TME consists of cells necessary for tumor sustenance or physical and mechanical support, including endothelial cells, macrophages, and cancer-associated fibroblasts. The tumor-associated vasculature plays an essential role in sustaining the tumor by transporting

nutrients and oxygen and eliminating catabolites. New vessels are formed by endothelial cells during a process known as the angiogenic switch, in which activation signals quiescent endothelial cells to proliferate and form new blood vessels. Cancer-associated fibroblasts (CAF) are cells with similarities to fibroblasts and myofibroblasts. The former secrete a variety of extracellular matrix components that provide the structural basis to support tumor growth, whereas the latter aid tumor cell proliferation, angiogenesis, invasion, and metastasis.

Immune cells are present in most, if not all, neoplastic lesions to the extent that they are included in the TME: infiltrating immune cells play a contrasting role, as they can perform both antagonistic and tumor-promoting functions. A pro-tumoral role has been attributed to tumor-associated macrophages (TAM) that suppress immune responses, activate fibroblasts, and promote angiogenesis[26].

The EV-mediated crosstalk between TME components and tumor cells strongly contribute to the establishment of conditions favorable to cancer growth and progression. A major effect promoted by EVs is the establishment of an immunosuppressive TME. EVs can carry immunomodulatory proteins, lipids and regulatory RNAs aimed at (i) suppressing T cell activation and proliferation, (ii) dampening NK cell cytotoxicity, (iii) inhibiting the maturation of Dendritic Cells (DCs), (iv) and functionally reprogramming macrophages.

2.4 The bone marrow metastatic niche in neuroblastoma

The main metastatic niche in HR-NB patients is the bone marrow (BM), the soft, spongy tissue within bone that is essential for hemopoiesis. NB cells infiltrating the BM establish complex interactions with resident cells, such as hematopoietic, endothelial, Schwann, and mesenchymal stromal cells, forming a dynamic and complex TME. BM-infiltrating tumor cells express NB-specific surface markers such as GD2 or B7-H3, which is the ligand of an inhibitory immune checkpoint receptor, and NB-specific mRNAs including TH and PHOX2B[27].

Cytomorphologic analysis of the BM smear under the microscope is the clinically approved technique to quantify BM infiltration: it allows to the identification of single or clustered NB cells, which are recognizable because they are typically round and larger than lymphocytes and have a high nuclear/cytoplasmic ratio[28].

The cellular composition of BM metastatic niche has been widely characterized[28]. Metastatic BM shows an increase in distinct cell populations fostering an immunosuppressive environment. This suppression is due to several mechanisms, including tumor-secreted cytokines and chemokines, elevated expression of immune checkpoint molecules, impaired natural killer (NK) cell function, and the infiltration of immunosuppressive cells such as tumor-associated macrophages (TAMs) and regulatory T cells (Tregs).

Within the myeloid lineage, an increased presence of immunosuppressive myeloid cells, including TAMs and tumor-associated neutrophils (TANs), is identified in metastatic BM samples. Additionally, a greater prevalence of exhausted cytotoxic T lymphocytes (CTLs) and dysfunctional NK cells is observed. Gene expression analysis of T and NK cells reveals higher expression of immune checkpoint molecules along with a decline in markers associated with cell activation[29].

It has been shown that NB-infiltrating BM samples are enriched of mesenchymal stromal cells (MSCs) showing functional alterations due to reduced clonogenic capacity, a shift toward osteogenic differentiation, and a reduction in the CD271+ clonogenic subset. These features reflect the stromal reprogramming observed in other BM-infiltrating malignancies and suggest that MSCs may exert pro-tumorigenic activity. The same study revealed a distinctive $CD146^{+}/CD271^{-}$ MSC subpopulation correlating with NB cell infiltration, potentially representing an immature, tumor-induced stromal phenotype. This hypothesis was further supported by its dynamics during therapy, as it disappeared in remission but re-emerged in progressive disease. Despite the specific function of this MSC subset is still unknown, its association with osteogenic programs and the known role of CD146 in tumor progression point out its relevance to metastatic niche maintenance and treatment resistance[30].

While several studies showed how the cellular composition in the BM metastatic niche can lead to an immunosuppressive TME, little is known about the immunosuppressive role of BM-derived EVs in NB patients. A recent study reported that both PD-L1 and HLA-G, a non-classical MHC class I molecule involved in immune tolerance, were expressed on the surface of BM-derived EVs, synergistically enhancing the secretion of immunosuppressive cytokines and inhibiting pro-inflammatory cytokines, resulting in the suppression of T-cell response and facilitating immune evasion[31].

The immunosuppressive TME hinders and limits the efficacy of immunotherapy with anti-GD2 monoclonal antibody, which is currently the standard of care for HR-NB patients.

As a deep investigation of BM-EVs is still lacking, the characterization of such vesicles and the assessment of EV-carried molecules contributing to the establishment of an immunosuppressive TME might help improving the current treatment and the development of novel therapeutic strategies aimed at enhancing immunotherapy response[32].

3. Aim of the Study

The aim of this study was to characterize sEVs derived from the BM of HR-NB patients, comparing patients with and without tumor infiltration and evaluating potential differences in the RNA expression profile, including mRNA, microRNA and long non-coding RNA. Indeed, dysregulated microRNAs may target biological pathways that contribute to a more aggressive tumor phenotype, such as the one observed in BM-infiltrating NB. We will determine in which biological pathways differentially expressed RNAs are involved, assessing their value as potential biomarkers and, thus therapeutic targets, for improving current therapeutic strategies.

4. Material and Methods

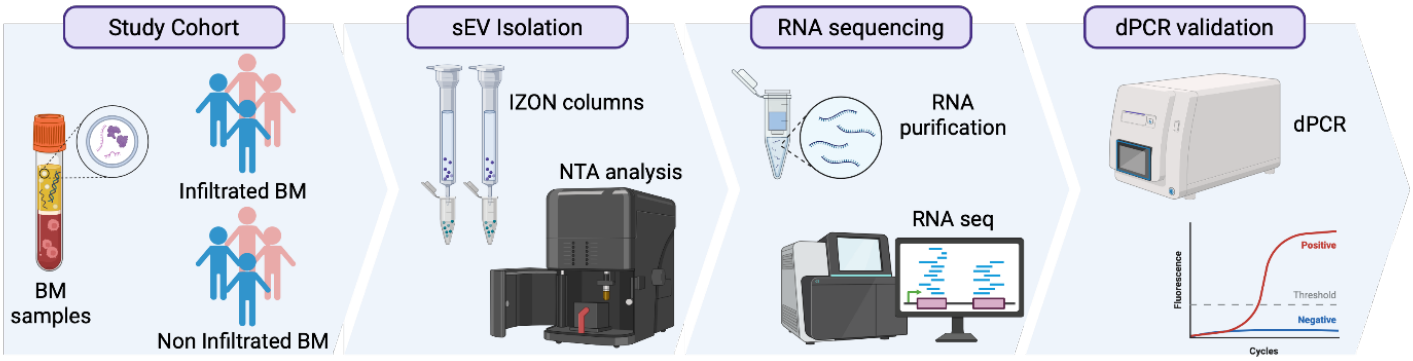

Figure 2: Graphical representation of the methodological workflow [made with BioRender.com].

4.1 Study cohort and patient clinical features

The study cohort included Italian HR-NB patients with (n=13) and without (n=14) BM infiltration. BM infiltration has been determined by cytomorphological evaluation and indicated with a value from 0 (no infiltration), to 3 (high degree of infiltration). Patient clinical features are reported in Table 2. All samples were collected from stage 4 HR-NB patients at diagnosis. The MYCN oncogene was amplified in 13 patients, and not amplified in 9 cases, while 3 patients had MYCN gain, a low-level copy number increase in the MYCN gene. MYCN status could not be determined for 2 patients. Concerning the follow-up data, 10 patients relapsed, while 17 patients did not report any progression or relapse. Finally, 16 patients had a favorable overall outcome, 19 deceased and for 2 of them data were not available.

Table 2. Patient clinical features

Clinical Features	Classification	Patients (n = 27)
Infiltration	0	14 (51 %)
	1	2 (8 %)
	2	6 (22 %)
	3	5 (19 %)
MYCN status	Amplified	13 (48 %)
	Not amplified	9 (33 %)
	MYCN Gain	3 (11 %)
	Not executed	2 (8 %)
Relapse	Yes	10 (37 %)
	No	17 (63 %)
Overall Survival	Alive	16 (59 %)
	Deceased	9 (33 %)
	Not available	2 (8 %)

Table 2: The table reports the main clinical features of the patients enrolled in the study: bone marrow infiltration, MYCN oncogene status, relapse and overall survival.

4.2 Bone marrow processing and biobanking

BM samples were processed and stored in the BIT-Gaslini Biobank, which centralizes the NB specimens derived from Italian AIEOP (Associazione Italiana Emato-Oncologia Pediatrica) centers. Written informed consent was signed from the parents or legal guardian of each patient considered for the study.

All samples were registered in XTENS 2.0, the web-based platform associated with the BIT-Gaslini Biobank. Samples were recorded and pseudonymized through a unique numerical code. The database stores sample-specific information recorded upon sample arrival: sampling date, arrival date, sample codification (plasma or bone marrow), pathology, sample quantity, city and hospital of patient recovery, tumor status, bone marrow infiltration.

BM samples were collected in EDTA tubes and processed within 24 h. Samples were centrifuged at 1200× g for 10 min at room temperature (RT) to collect plasma. Plasma was stored at −80 °C or used immediately for sEVs isolation. BM processing according to the BIT-Gaslini Biobank standard operating procedures (SOPs) ensured homogeneity in sample preparation, resulting in high-quality biological specimens to be used for downstream analysis.

4.3 sEV isolation for morphological characterization

Small EV isolation was performed starting from 500 µl of plasma by using qEVoriginal 35nm GEN2 columns (Izon Science), a method based on size-exclusion chromatography principle. The column is

filled with porous microspheres that act like a molecular sieve: large molecules (in this case, sEVs) cannot enter the pores and therefore pass quickly, while small molecules (in this case, proteins) diffuse into pores and subsequently elute. Figure 3 shows the volume fractions containing eluted sEVs according to manufacturer instructions.

Plasma samples were centrifuged at 13,200 x g for 10 minutes at 4°C to remove any cellular debris. Columns were equilibrated with 17 ml PBS before loading plasma samples. 500 µl of sample were loaded into the columns and 2.5 ml PBS were added and collected as void volume. The sEVs were then progressively eluted with PBS in 5 fractions of 0.4 ml each. The columns were washed with a solution of sodium hydroxide 0.5 M and 17 ml PBS and then stored in buffer with 0.05% of sodium azide at 4°C.

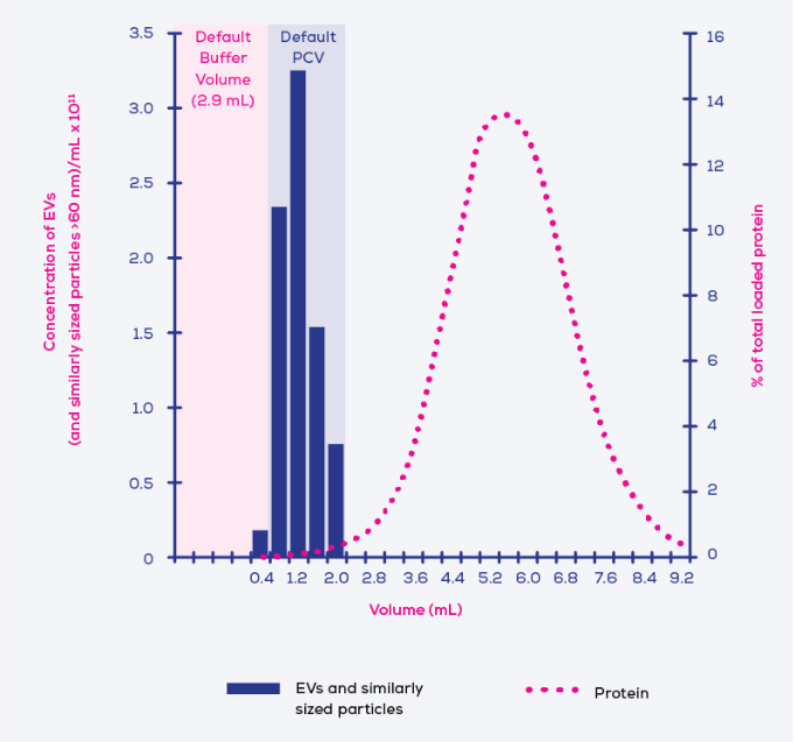

Figure 3: Elution profile of sEVs with the qEV IZON columns.

sss are eluted in volumes ranging from 0.4 to 2.0 ml. Volumes above 2 ml contain proteins. Elution volumes are reported on the X axis, while the expected concentration of sEVs is shown on the Y axis. Dotted line represents protein contamination.

4.4 EV characterization

4.4.1 Concentration of EVs

The eluted fractions were pulled together and isolated sEVs were concentrated using Amicon® Ultra-4 10K: devices, equipped with an internal membrane that blocks the passage of sEVs.
Amicon columns were normalized with 4 ml of PBS and centrifuged at 1000 x g for 5 minutes at RT. sEV eluted samples were loaded on the membrane and centrifuged at 1800 x g for 8 minutes at RT. The concentrated samples were collected with a pipette directly from the membrane.

4.4.2 Transmission Electron Microscopy Analysis

Transmission electron microscopy (TEM) is the most commonly employed technique to characterize sEV morphology. Isolated sEVS were sent to Professor Katia Cortese (Dipartimento di Medicina Sperimentale, Genova) to perform morphology analysis. Briefly, 5µl drops of purified sEVs were placed onto grids and adsorbed for 20 min at room temperature. Grids were fixed in 4% PFA in PBS pH 7.2 for 5 min. Contrast enhancement was obtained by further incubating the grids with 2% uranyl acetate for 5 min. After drying, grids were immediately observed with a Hitachi 7800 120kV (Hitachi High-Tech). Digital images were taken with a Megaview III camera and acquired with Radius software.

4.4.3 Zetasizer Qualitative Analysis

To determine the size distribution EVs in suspension, the samples were analyzed by Zetasizer Nano Instrument (Malvern). It is based on Dynamic Light Scattering (DLS), which measures scattered light from particles undergoing Brownian motion. The dynamic information is traced and converted. Specifically, samples were diluted 1:2 (25 µl of sample + 25 µl of PBS) and analyzed in disposable cuvettes. Size distribution results can be reported in graphs reporting intensity distribution, volume distribution, and number distribution. Intensity measurement is based on the light scattering intensity of particles, which is proportional to their size: larger particles scatter more light. Intensity data are converted into an estimation of particle volume: volume distribution considers the relative mass or volume of particles. Finally, the number distribution estimates the count of particles in each size range. The polydisperse index (PDI) is indicative of the size homogeneity of sEVs: the lower the PDI value, the more homogeneous the sEV population.

4.4.4 Nanoparticle Tracking Analysis

To determine the quantity of isolated sEVs, Nanoparticle tracking analysis (NTA) was performed. NTA determines the concentration of sEVs in the sample (particles/mL). The particles in the sample move according to Brownian motion; the motion can be captured by the camera once the particles are

illuminated by light as each particle scatters light differently. Samples were diluted 1:500 (2 µl of samples + 2 ml of PBS) and analyzed with NanoSight NS300 (Malvern).
NTA provides real-time video tracking of nanoparticles, allowing researchers to visually confirm particles presence in the sample before analysis starts. The most important data provided by NTA is the total particle concentration per volume of liquid (particles/ml). In addition, it reports a size distribution graph that shows the range and frequency of different particle sizes.

4.5 sEV isolation for RNA purification

The exoRNeasy Midi kit (QIAGEN) was used both to isolate sEVs from 500 µl of plasma and to purify RNA. The system relies on a membrane affinity binding step to isolate sEVs, exploiting their generic biochemical features. Membrane-attached sEVs are treated with QIAzol Lysis Reagent, which lyses the lipid membrane and favors the removal of proteins, RNases and DNA to selectively collect EV-RNA.
Plasma samples were centrifuged at 13,200 x g for 10 minutes at 4°C to remove any cellular debris. The purified samples were diluted 1:2 with XBP buffer (500 µl of plasma + 500 µl of XBP buffer) and thoroughly homogenized by inversion. The entire volume was loaded into the exoRNeasy column and centrifuged at 500 x g for 1 min at RT to allow sEVs to attach to the column filter.
The flow-through was removed, and to wash the sEVs 3.5 ml of XWP buffer were loaded into the column and centrifuged at 5,000 x g for 5 minutes at RT. The flow-through was discarded, and after changing the collection tube, sEVs attached to the filter were lysed with 700 µl of Qiazol. A final centrifugation step at 5,000 x g for 5 minutes at RT allowed the collection of the lysate.

4.6 RNA extraction from sEVs

Total sEV-RNA was extracted by using the exoRNeasy Midi kit (QIAGEN). 90 µl of chloroform was added to the lysate, the volume was thoroughly mixed, after 2-3 minutes the samples were mixed again and centrifuged at 12,000 x g for 15 minutes at 4°C. After centrifugation, two distinct phases are visible: the aqueous phase containing nucleic acid, above the white ring of proteins, was collected. Two volumes of ethanol 100% were added to the aqueous phase. The entire volume was loaded into the RNeasy MinElute column and centrifuged at 12,000 x g for 15 seconds at RT (RNeasy MinElute columns contain a maximum volume of 700 µl: this step was repeated until the sample was exhausted). Wash steps were performed with 700 µl of RWT followed by 500 µl of RPE by centrifuging the samples at 12,000 x g for 15 seconds at RT. A further wash was performed with 500 µl of RPE by centrifuging the samples for 2 minutes. Samples were centrifuged dry for 5 minutes at

RT. Finally, RNA was eluted with 19 µl of RNase-free water and collected in a new collection tube after centrifugation at 12,000 x g for 1 minute at RT.

4.7 Quantitative sEV-RNA analysis and miRNA fraction assessment

RNA was quantified with the Qubit™ 4 system (Thermo Fisher Scientific), a microvolume fluorometer that measures the signal intensity of fluorescent dyes bound to nucleic acids. The concentration of RNA in the sample (ng/µl) is calculated by comparing its relative fluorescence units (RFU) with the RFU of standard samples. The calibration curve is created by using standard samples. As we started from a very low volume of plasma samples, the RNA quantification was performed with the high sensitivity (HS) RNA assay: 1 µl of sample is mixed with 199 µl of working solution, consisting of 1 µl dye and 199 µl of buffer.

To assess the presence of a significant microRNA fraction within the purified RNA, the Small RNA Assay run on the Agilent 2100 Bioanalyzer (Agilent Technologies) was performed. The Small RNA assay is based on microfluidic capillary electrophoresis technology to resolve low abundant nucleic acid in the size range of 6 to 150 nucleotides. Total RNA molecules are separated by size as they pass through a network of microchannels within a chip. Detection relies on the fluorescence emitted by an RNA-bound intercalating dye, generating an electropherogram that visualizes RNA fragment distribution according to their retention time. The instrument software converts retention time data into nucleotide number of the RNA fragments, using a ladder as a reference.

4.8 RNA sequencing and data analysis

sEV-RNA samples were sent to IGA Technology Services (Udine,Italy) to perform total RNA sequencing analysis. An amount of 100 ng of RNA was provided for each sample. Two different libraries, one for total RNA and another for small RNA were prepared.

Raw data from next generation sequencing of biological samples (Fastq files) were pre-processed and aligned to the human reference sequence to obtain an expression matrix, with targets as rows and samples as columns. Nf-core/rna-seq pipeline (_https://github.com/nf-core/rnaseq) was used to pre-process and align raw RNAseq Fastq files on the hg38 reference sequence, in particular UMI based deduplication on STAR aligned bam files was used to remove PCR duplicates before gene counts estimation by Salmon. Paired reads obtained after deduplication were used as input for LncPipe, a nextflow pipeline for the evaluation on LncRNA expression from RNAseq.

miRNA Fastq were processed with MIRGE3.0 software[33]. Differential gene, miRNA and long non-coding RNA expression analysis between patients with and without BM infiltration was conducted with SAM (significance analysis of microarrays)[34]. The most variable genes, miRNAs, and lncRNA,

considering the median absolute deviation (MAD) were integrated with Movics, a data integration R package[35].

4.9 microRNA sequencing data validation by digital PCR

Data obtained with high-throughput RNA sequencing technology need to be validated with accurate methods to confirm the biological variability observed. To this end, we selected digital PCR (dPCR), a highly sensitive technique enabling the quantification of low abundant targets. The method is based on the compartmentalization principle: partitioning DNA samples into thousands of individual reactions, each with a low number of target molecules as shown in Figure 4, allows an accurate and absolute quantification without the need either of a standard curve or a reference. The analysis is based on Poisson statistics to determine the probability of the target distribution during partitioning.

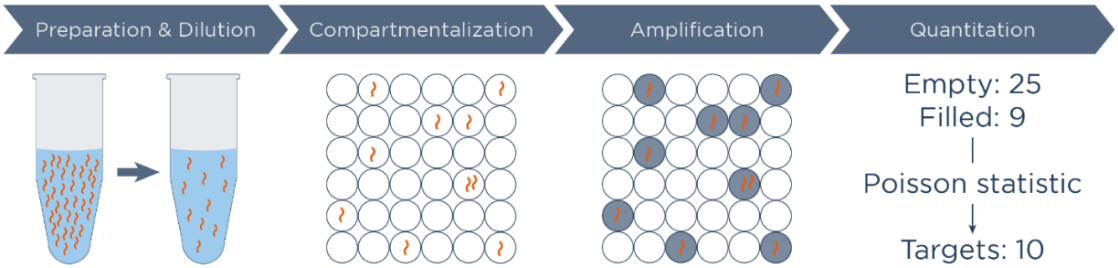

Figure 4: Graphical workflow of dPCR [www.actome.de].

4.9.1 Reverse transcription

RNA samples were reverse transcribed into cDNA using the TaqMan® microRNA Reverse Transcription Kit (Thermo Fisher Scientific), which allows to specifically reverse transcribe microRNAs. Specifically, 50 ng of samples were reverse transcribed in a maximum volume of 3 µl, and 4.5 µl of reverse transcription mix were added for each sample. Mix composition per sample: 0.80 µl of Megaplex RT Human Pool A primer (10X), 0.20 µl of deoxynucleoside triphosphates (dNTPs) with deoxythymidine triphosphate (dTTP), 1.50 µl of multiscribe reverse transcriptase, 0.80 µl of RT buffer (10X), 0.90 µl of $MgCl_2$, 0.10 µl of RNase inhibitor, 0.20 µl of H_2O RNase-free.
Reverse transcription program: after an initial step of 2 minutes at 16° C, program executes 40 cycles of 1 minute at 42° C for primer annealing, followed by 1 second at 50° C for transcript elongation. The program ends with an enzyme inactivation step performed at 85°C for 5 minutes. Finally, the temperature is maintained at 4° to preserve integrity of sample until it is extracted from the instrument.

4.9.2 Pre-amplification

cDNA samples were pre-amplified using Megaplex™ PreAmp Primers Human Pool Set v2.0 kit (Thermo Fisher Scientific) to ensure sufficient material for digital PCR analysis. 2.5 µl of cDNA sample was pre-amplified in a total volume of 25 µl. Mix composition per sample: 12.5 µl of TaqMan pre-amp Master Mix, 2.5 µl of Megaplex pre-amp primers Human Pool A and 7.5 µl of H_2O RNase-free.

Pre-amplification program: the initial cDNA denaturation 10 minutes at 95° C was followed by primer annealing 2 minutes at 55 °C and elongation 2 minutes at 72 °C. After these 3 steps, 12 cycles of denaturation 15 seconds at 95 °C, and combined primers annealing and elongation phase 4 minutes at 60 °C followed. Program ended with 10 minutes at 99.9 °C for fine denaturation. Finally, the temperature was maintained at 4° to preserve integrity of sample until it is removed from the instrument. At the end of pre-amplification program, 75 µl of H_2O RNase-free were added to each sample to reach a final volume of 100 µl.

4.9.3 Digital PCR assay

Pre-amplified cDNA samples were quantified using QIAcuity Probe PCR Kit 4X (QIAGEN) and TaqMan microRNA Primer Assay 20X (Thermo Fisher Scientific). 1 µl of cDNA was quantified in a total volume of 40 µl. The final mix composition was made of QIAcuity probe 1X, TaqMan microRNA Primer Assay 1X and H2O RNase-free. Samples were prepared in a pre-plate; volume of each well was transferred in Nanoplate 26K 24-well plate which is then sealed with foil.

Samples were analyzed with the QIAcuity One digital PCR system (QIAGEN) with the following steps: 10 minutes at 95° C for cDNA denaturation, 40 cycles of 15 seconds at 95 °C, for new synthesized DNA fragments denaturation, and 30 seconds at 60 °C for combined primers annealing and elongation phase. Acquisition was performed using 500 ms exposure time and a gain value of 1.

4.10 Statistical analysis

Differentially expressed RNA species were detected with deseq2, and only RNA targets with p-value adjusted for multiple testing by deseq2 model <0.05 were considered significant[36].

For gene targets, the enrichment analysis was based on hypergeometric test after adjustment for false discovery rate (FDR), while for miRNAs and lncRNAs the unbiased empirical sampling-based approach was applied.

In ROC analysis, the AUC standard error (SE) was calculated with the method DeLong et al.[37], and the confidence interval was calculated as AUC ± its SE.

To calculate the significance of the differential expression measured by dPCR, unpaired T-test was applied.

5. Results

5.1 Characterization of sEVs derived from BM samples of HR-NB patients

To isolate and characterize sEVs from BM of NB patients we used a size-exclusion chromatography (SEC)-based method, allowing to preserve vesicle structure and integrity. Qualitative assessment with both TEM and Zetasizer analyses showed consistent results, indicating that that the average diameter size of isolated EVs ranged between 100-160 nm.

We performed TEM analyses on sEVs isolated from BM (Figure 5, right) and PB samples (Figure 5, left). sEVs (indicated by red arrows in Figure 5) appear as dark dots of uniform size with a diameter of approximately 100 nm. The shape of the sEVs is perfectly round and fragments aren't visible in the sample: the isolation method used is suitable for the subsequent qualitative and quantitative analyses of sEVs, as their morphological structure is retained. Despite the presence of aggregates due to the complex nature of patient-derived biological specimens, sEVs are present in higher concentration than background fragments.

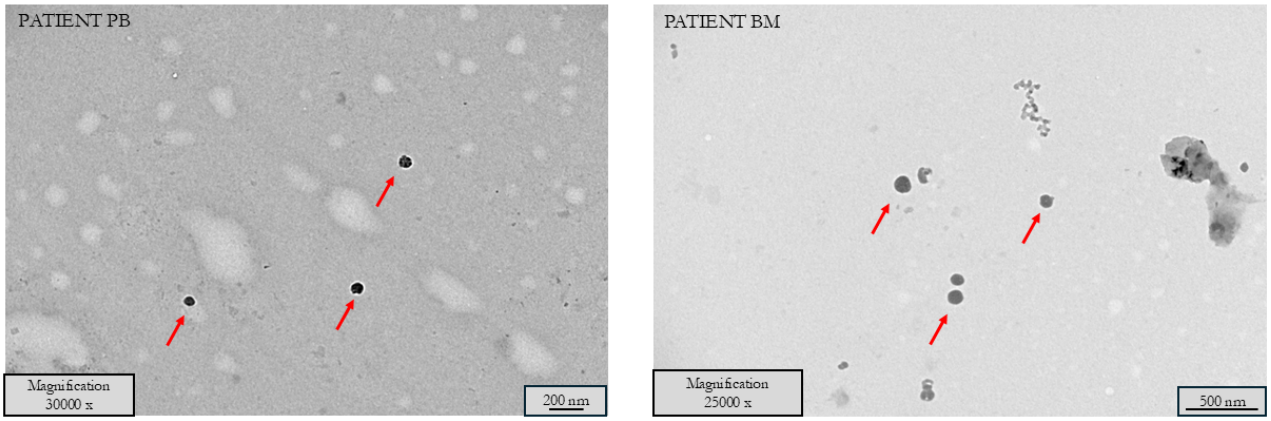

Figure 5: sEVs morphological characterization. Transmission electron microscopy acquisition of sEVs isolated from peripheral blood (left) and bone marrow (right). Magnification settled at 30,000 x for image on the left and 25,000 for image on the right. Scale bars are reported at the bottom right of each image.

We performed the same comparison between matched PB and BM infiltrated (BM pos) and non-infiltrated (BM neg) samples with Zetasizer. Quality report was good for all samples, suggesting the efficiency of the isolation method and the reliability of data. sEV size was reported as Z-Average: the average hydrodynamic dimension that considers the intensity with which each particle scatters light. Figure 6 shows two representative Zetasizer analysis of two NB patients of our study cohort. We could not detect any significant difference in the diameter size of sEVs either between PB (Figure 6 panels A and C) and matched BM neg (Figure 6B) or pos (Figure 6D) samples, and between BM pos and BM neg samples (Figure 6 panels B and D). As reported in Table 3, the sEVs have an average diameter ranging between 144.7-158.8 nm. The PDI value, indicative of vesicle size homogeneity, was also reported in Table 3. The PDI of PB and BM in non-infiltrated patients is very similar and

has a good value of 0.336-0.353, while in infiltrated patients, the PDI slightly differs between the two sources, 0.468 in PB to 0.298 in BM. However, considering the complex biological source of sEVs, PDI values <0.5 are indicative of a good degree of homogeneity of the isolated vesicles.

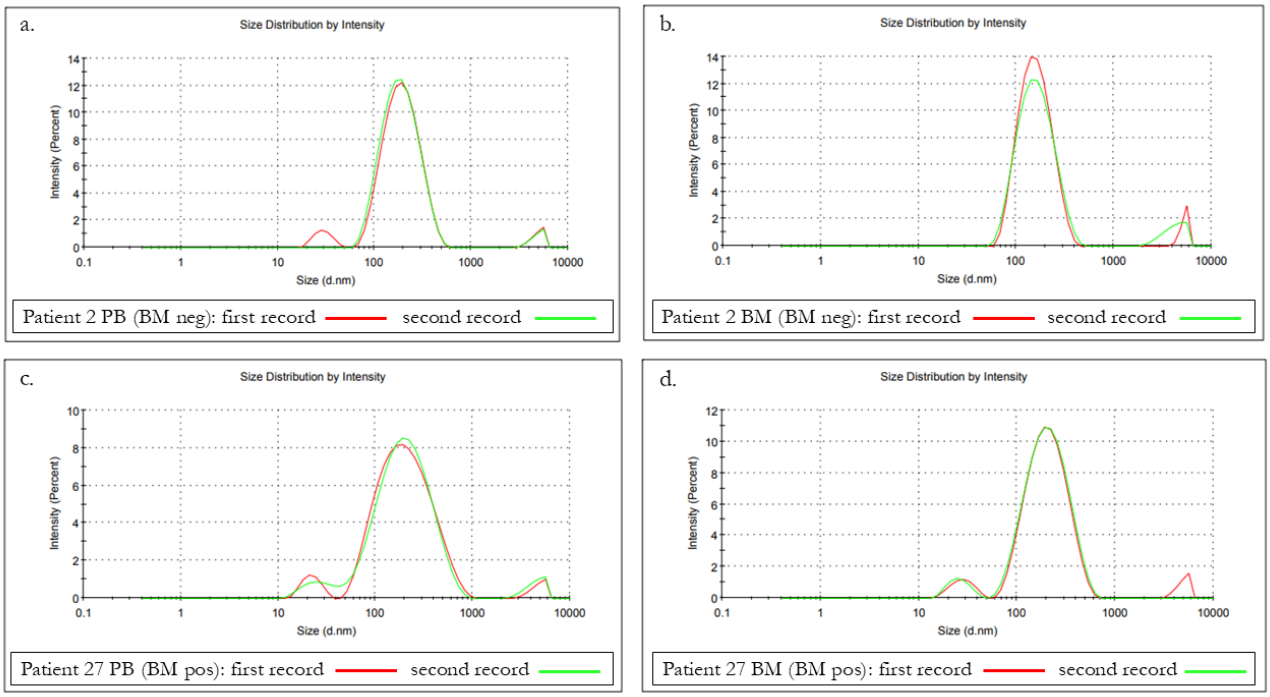

Figure 6: sEV size distribution analysis with Zetasizer Nano instrument. Panels a–b show peripheral blood (PB) and bone marrow (BM) analyses, respectively, of the BM-negative patient. Panels c–d show the corresponding analyses of the BM-positive patient. Two measurements (represented by the red and green lines) are displayed for each sample. The X-axis indicates particle diameter in nanometers, while the Y-axis shows sample intensity, expressed in percentage relative to the highest peak, normalized to 100%.

	Patient 2 BM neg		**Patient 27 BM pos**	
	PB	BM	PB	BM
Z-Average (nm)	158.8	144.7	147.7	155.0
PDI	0.336	0.353	0.468	0.298

Table 3: Summary of Zetasizer values related to size analysis of sEVs. Table columns correspond to BM–non-infiltrated (BM neg) and BM–infiltrated (BM pos) patients, with separate data for peripheral blood (PB) and bone marrow (BM) samples. Table rows report the particles' Z-Average (expressed in nanometers) and the polydispersity index (PDI).

The overall results of the whole cohort are reported in Table 4. Non-infiltrated NB patients reported an average EV diameter size of 137.2 ± 5.84 nm and a PDI of 0.268 ± 0.024 for PB, and a diameter size of 132.7 ± 5.75 nm and a PDI of 0.274 ± 0.016 for BM. Infiltrated NB patients showed an average EV diameter size of 145.3 ± 5.57 nm and a PDI of 0.228 ± 0.011 for PB, and a diameter size of 134.2 ± 4.25 and a PDI of 0.308 ± 0.012 for BM.

	PB neg	BM neg	PB pos	BM pos
Z-Average (nm)	137.2 ± 5.84	132.7 ± 5.75	145.3 ± 5.57	134.2 ± 4.25
PDI	0.268 ± 0.024	0.274 ± 0.016	0.228 ± 0.011	0.308 ± 0.012

Table 4: Summary of Zetasizer analysis. The table show the mean value of size (nm), expressed as Z-Average, and PDI in the whole study cohort. Columns refers to non-infiltrated (PB neg, BM neg) and infiltrated (PB pos, BM pos) patient samples. PB=peripheral blood; BM=bone marrow. Values are expressed as average ± standard error.

Qualitative analyses were further confirmed by NTA analysis (Figure 7), which also provides quantitative results. Vesicle size in NTA was expressed both with mode and mean as shown in Table 5: the mode value was between 96.9 nm and 113.3 nm, while the average values were slightly higher and consistent with the values obtained by Zetasizer analysis, ranging between 132.0 nm and 137.6 nm.

Table 5 reports sEVs concentration as mean value +/- standard error: the range of concentration is similar in PB and BM in both BM-positive and BM-negative patients. A lower concentration of 1.25 x 10^{11} ± 7.29 x 10^{9} particles/ml was observed in PB of not-infiltrated patients compared with PB of BM-infiltrated patients (1.63 x 10^{11} ± 5.06 10^{9} particles/ml).

Considering the limit of biological sampling in pediatric patients, these data support the efficacy of the SEC-based isolation method in yielding a considerable number of vesicles from a starting volume as low as 500 µl of plasma. Moreover, the isolated sEV population was homogeneous in terms of size in both PB and BM samples, with the latter showing a higher concentration of sEVs compared to matched PB samples.

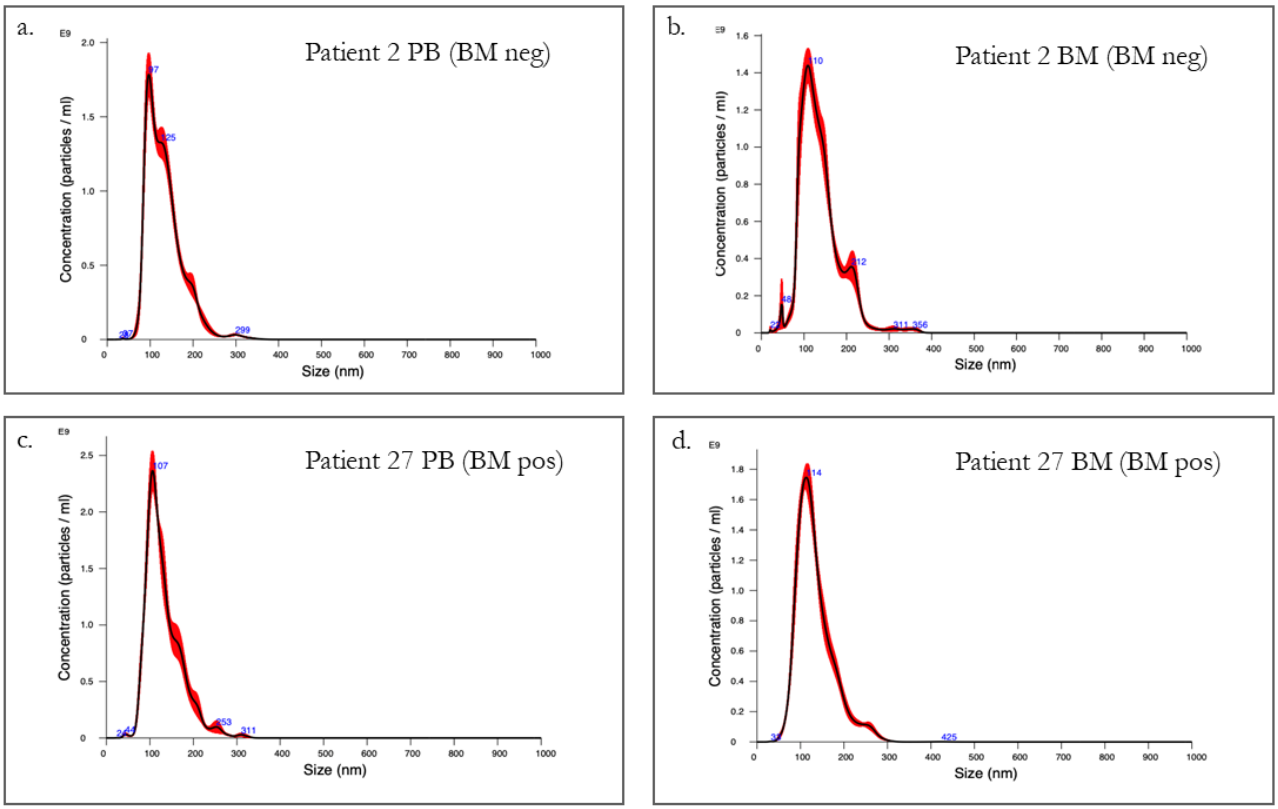

Figure 7: sEV size distribution and concentration analysis with NanoSight NS300 (Malvern). Panels a and b show peripheral blood (PB) and bone marrow (BM) analyses, respectively, of the BM-negative patient. Panels c–d show the corresponding analyses of the BM-positive patient. The red line represents the merged data from all replicates, while the black line corresponds to the mean of the replicates. The blue numbers indicate the exact size of the particles that fall within the peaks in the graph. The X-axis indicates particle diameter in nanometers, while the Y-axis shows sample concentration in particles/ml.

	Patient 2 BM neg		**Patient 27 BM pos**	
	PB	BM	PB	BM
Mean Size (nm)	137.6	133.1	132.0	133.9
Mode Size (nm)	109.3	96.9	106.1	113.3
Concentration (particles/ml)	$1.25 \times 10^{11} \pm 7.29 \times 10^{9}$	$1.35 \times 10^{11} \pm 5.82 \times 10^{9}$	$1.63 \times 10^{11} \pm 5.06 \times 10^{9}$	$1.40 \times 10^{11} \pm 3.29 \times 10^{9}$

Table 5: Summary of Nanoparticle Trafficking Analysis values related to size and concentration analysis of sEVs. Columns correspond to BM–non-infiltrated (BM neg) and BM–infiltrated (BM pos) patients, with separate data for peripheral blood (PB) and bone marrow (BM) samples. Table rows report particle diameter size indicated as mean and mode (expressed in nanometers) and particle concentration (expressed in particles/ml).

5.2 sEV-RNA quantity and quality were suitable for RNA sequencing

To perform RNA sequencing, 100 ng of RNA for each sample were supplied to IGA Technology Services (Udine). The Qubit™ 4 system is a more sensitive quantification assay method than spectrometer-based techniques. For optimal sequencing, it is essential to know the RNA concentration thus, Qubit quantification of RNA purified from of all the patients included in our study cohort was performed. At least 100 ng of RNA was extracted from each sample, as shown in Figure 8. We were able to isolate EV-RNA between 100 and 600 ng for more than half of the patients (67%), and for the remaining samples (33%) we could obtain EV RNA yield higher than 600 ng, thus ensuring enough material for downstream analyses.

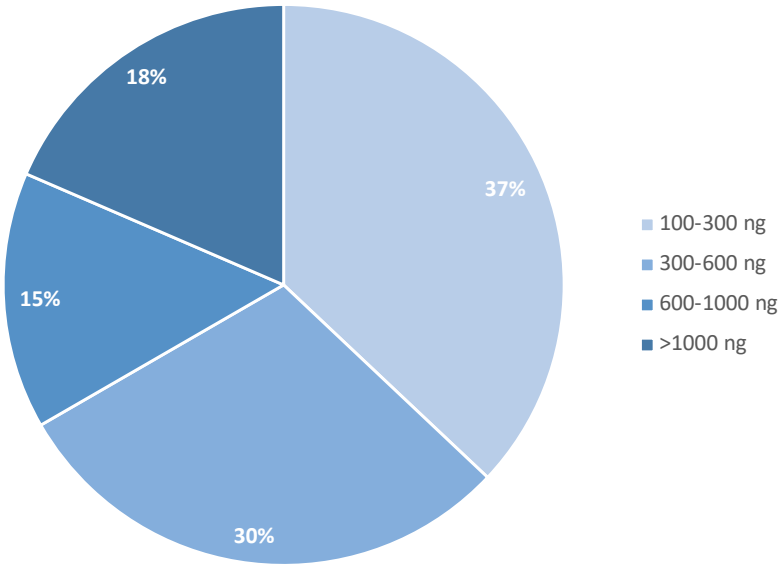

Figure 8: RNA concentration analysis. The graph illustrates the total RNA yield obtained for all the samples of the whole study cohort.

As ribosomal RNA is not carried by EVs, we could not perform the Nano RNA Assay on Agilent 2100 Bioanalyzer to assess RNA quality. However, we assessed the microRNA fraction of all the isolated EV-RNA samples by running the Small RNA Assay. Figure 9 shows the exemplifying results of sEV-miRNA profiling from patients with and without BM infiltration. The analyzed samples were enriched in microRNA fraction, as confirmed by the peaks observed between the two green dotted lines, corresponding to fragments 4 to 40 nucleotides long.

The height and width of the electropherogram's main peak (Figure 9) give important information about the quantity and homogeneity in size of the fragments. In both samples, the fluorescent signal was high, indicating a good amount of extracted microRNA. The narrower peak observed in the non-infiltrated BM sample falls mainly in the range of microRNAs, while the broader peak distribution observed in the infiltrated BM sample indicates an abundant concentration of microRNAs, but also a higher concentration of small-RNAs.

This information was confirmed by the image of the electrophoretic run (Figure 9): the thickness of the band provides information on the quantity of material, while its resolution indicates the homogeneity of the sample in terms of fragment size. The band of non-infiltrated sample was rather thick and well defined, indicating a good quantity and higher homogeneity, respectively. In the run of infiltrated sample, a rather thick band was visible but not well-resolved: the presence of several overlapping bands confirmed the greater heterogeneity of the sample due to the higher amount of small-RNAs.

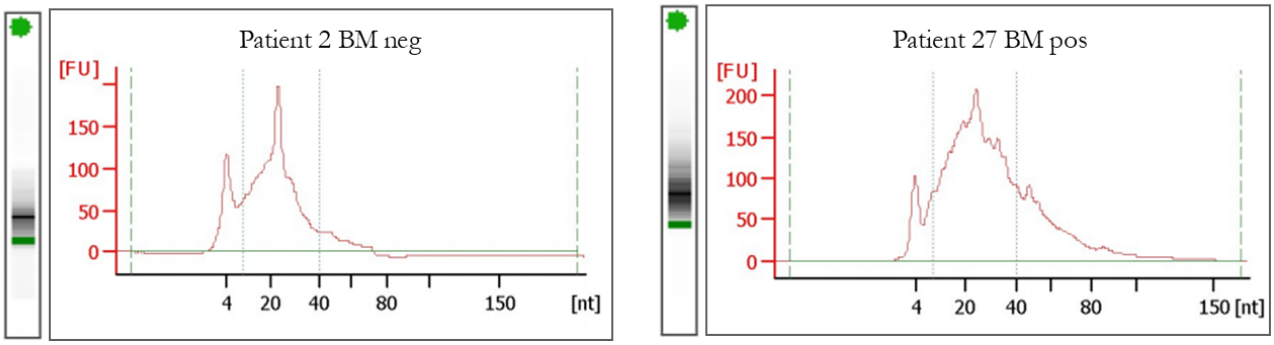

Figure 9: Analysis of RNA fragment size using the Agilent 2100 Bioanalyzer. Exemplifying graphs resulting from the capillary electrophoresis and the corresponding electropherogram are shown. The graph on the left displays RNA extracted from sEVs isolated from a non-infiltrated BM sample, while the graph on the right shows RNA extracted from an infiltrated BM sample. The X-axis represents RNA fragment size expressed in nucleotides, while the Y-axis indicates fluorescence intensity expressed in fluorescence units (FU) emitted by the RNA-interacting dye. The green dotted lines on the right of the graphs represent the limit of 150 nucleotide length for small RNAs, while the two dotted green lines indicate the microRNA size range.

5.3 BM-derived sEV from NB patients with BM infiltration showed a different RNA profile compared to non-infiltrated samples.

Total and small RNA sequencing was performed to evaluate miRNA content of sEVs, and subsequently differential expression analysis (DEA) was performed to highlight significant differences in expression (Mann-Whitney Test p-value <0.05) between NB patients with and without BM infiltration.

We observed the upregulation of 313 genes in BM-infiltrated samples. We performed pathway analysis (PA) to have insights in which biological pathways might be modulated due to NB cell infiltration. PA results showed the enrichment of biological processes involved in cell metabolism, signaling, immune response, growth and development, renal function and endocytosis and trafficking (Figure 10). While the modulation of mRNA targets in infiltrated BM samples did not reach the statistical significance, the differential expression we observed in terms of miRNA and lncRNA was significant.

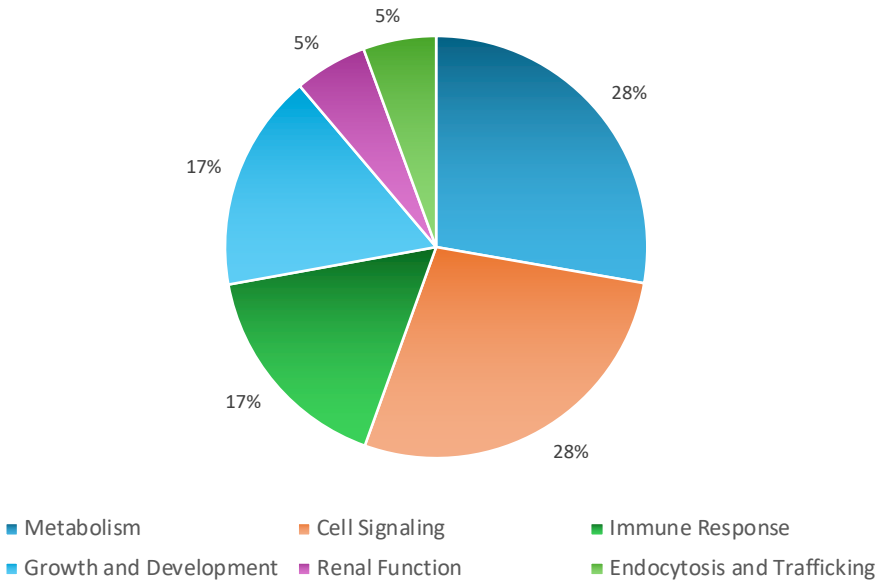

Figure 10: Enriched biological pathways targeted by mRNAs. The graph reports the main cellular biological categories resulted from miRNet analysis.

5.3.1 BM infiltrated NB patients showed the modulation of sEV-miRNA and sEV-lncRNA potentially involved in immune response

The most significant differentially expressed sEV-miRNA between BM infiltrated and non-infiltrated specimens were reported in Figure 11. The graphical visualization with heatmaps allows rapid understanding of global expression patterns and relationships between variables and samples. In the heatmap, each column represents a patient, and each row corresponds to a specific miRNA. Expression values were reported as Z-scores, reflecting the deviation of each patient's expression level from the average across all patients. Normalized values were converted to a color scale: white color indicates no deviation from the mean value, while red and blue correspond to higher and lower expression levels, respectively.

Notably, miRNA expression was predominantly downregulated in BM-infiltrated patients compared to non-infiltrated ones. Despite the heterogeneity of patient-derived biological material, clear patterns of differential expression were observed. To assess whether the downregulation pattern in BM-infiltrated patients may impair RNA interference mechanism, potentially leading to the upregulation of genes that support tumor progression, pathway analysis was performed.

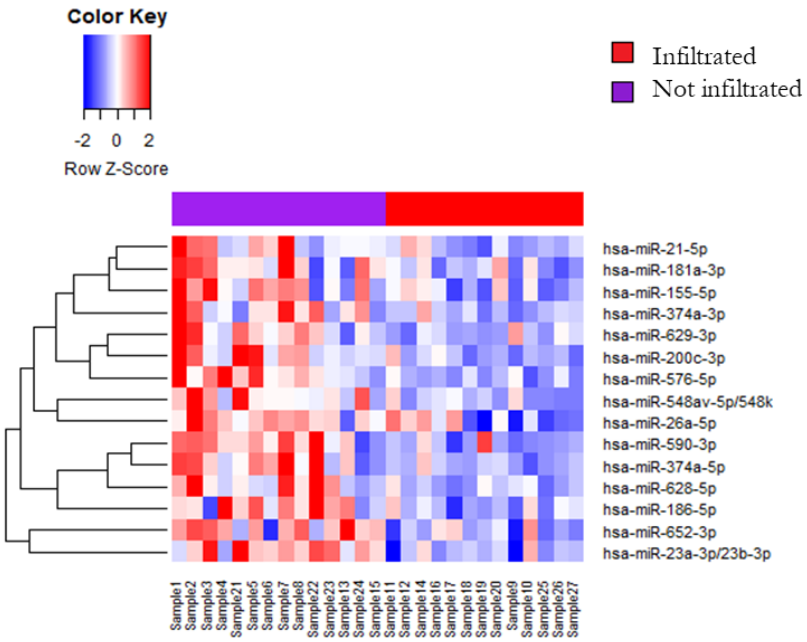

Figure 11: Heatmap of sEV-miRNA differential expression analysis between BM–infiltrated and non-infiltrated patients. Non-infiltrated patients are represented with purple bar, while the red bar indicates BM-infiltrated patients. Each column represents a patient, and each row corresponds to a specific miRNA. Expression values are reported as Z-scores and visualized using a color scale, with blue indicating downregulation and red indicating upregulation relative to the mean.

To this purpose, the potential biological targets of identified miRNAs were assessed through miRNet, a web-based tool for the functional analysis of miRNA networks, enabling to explore the interactions between miRNAs and other biological entities through interactive, network-based visualizations. To build the miRNA–target gene interaction network, miRNet relies on miRTarBase v9.0, a database of experimentally validated miRNA–target gene interactions, and TarBase v9.0, a comprehensive repository of experimentally supported miRNA–mRNA interactions. A degree filter with a cutoff of 3 was applied to highlight commonly shared targets. Functional enrichment analysis was executed on the generated network to identify associated biological pathways, using the Kyoto Encyclopedia of Genes and Genomes (KEGG) as the reference database.

miRNet identified 73 pathways with significant adjusted P value (adjP value < 0.05) divided into nine main biological groups reported in the diagram shown in Figure 12: Receptor tyrosine kinase signaling, apoptosis, PI3K-Akt and growth factor signaling, NOTCH signaling pathway, Wnt/β catenin pathway, gene regulation and DNA repair, immune signaling, senescence and stress response, hypoxia response. Immune signaling category included the B cell receptor signaling for the B cell activation and DAP12 signaling, which plays a critical regulatory role for the activation of several immune cell populations such as NK cells, monocytes, macrophages, and dendritic cells[38].

The activity of modulated sEV-miRNA in regulating immune response was further suggested by the enrichment of NOTCH and PI3K/Akt signaling pathways. The former is essential for the development and function of T cells, myeloid cells and NK cells[39]; the latter can promote the evasion of immune surveillance by suppressing T cell activity and enhancing cancer cell survival[40].

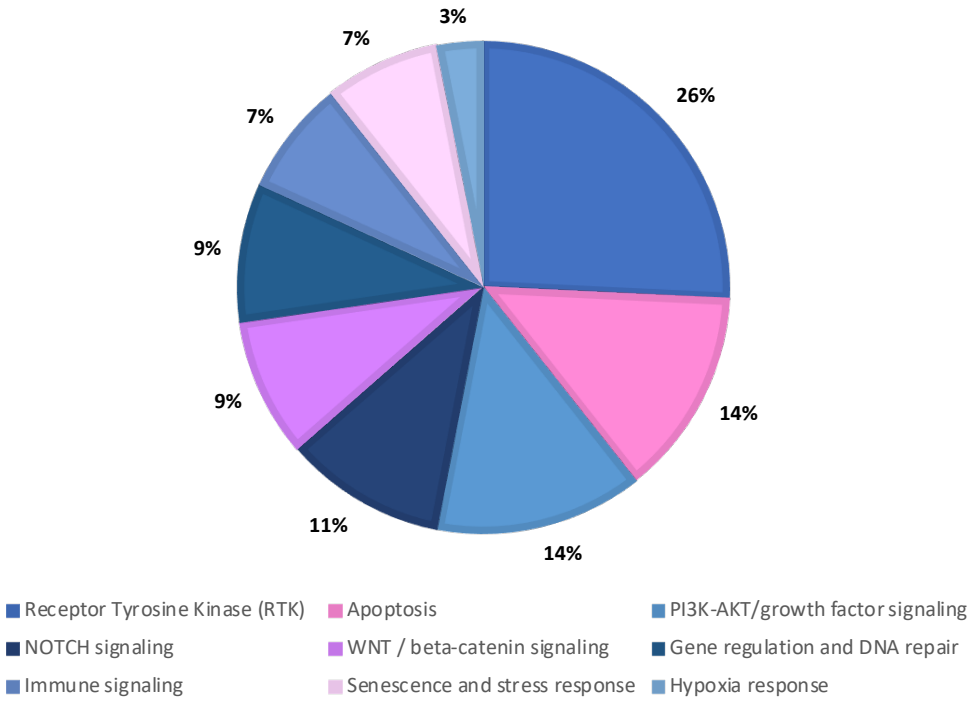

Figure 12: Enriched biological pathways targeted by microRNAs. The graph reports the main cellular biological categories resulted from miRNet analysis.

Differential expression analysis also revealed the modulation of sEV-lncRNA, as reported in Figure 13 A. Heatmap was built as previously described, showing the most significant lncRNA differentially expressed between infiltrated and non-infiltrated BM samples. We identified a list of 36 lncRNA and 116 lncRNA up and downregulated in NB patients with BM infiltration, respectively. To evaluate which biological pathways could be affected by the modulation of these lncRNA we performed PA by using miRNet tool, setting the cutoff of 3 to highlight commonly shared targets and identifying biological processes according to KEGG classification. Enriched pathways with significant adjusted P value (adjP value < 0.05) were grouped into main biological categories as reported in Figure 13 B. We observed that the modulated sEV-lncRNAs were mainly involved in immune system process, signal transduction, gene expression regulation, apoptotic process, cytoskeleton organization, developmental process, cellular senescence and stress response and vesicle-mediated transport.

These results, partially overlapping with the PA analysis reported for sEV-miRNA, highlighted that sEV small RNAs differentially expressed between infiltrated and non-infiltrated BM specimens could

strongly affect the immune response of HR-NB patients, thus potentially contributing to the immunosuppressive TME described in the BM metastatic niche.

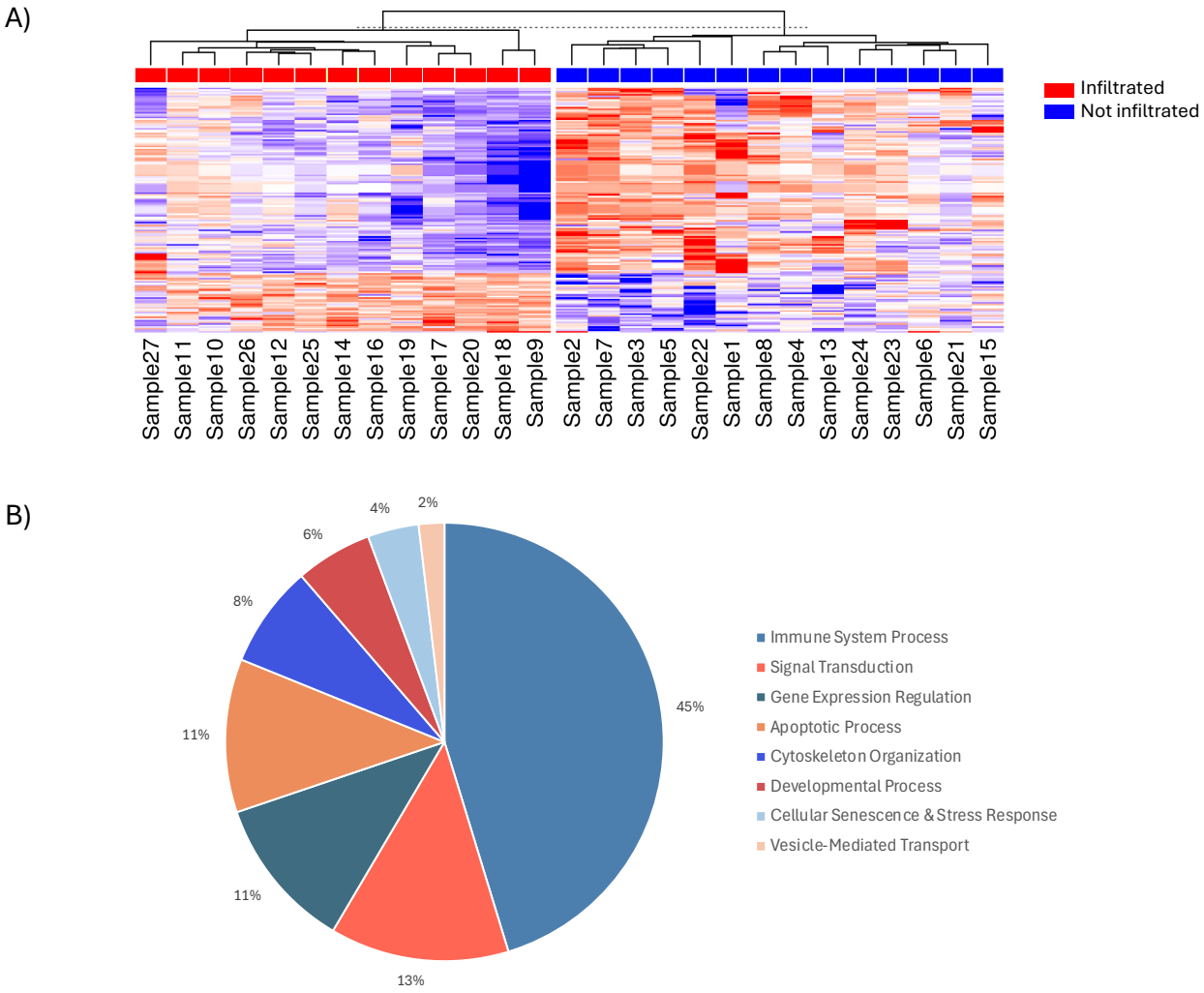

Figure 13: Differential sEV-lncRNA expression in BM samples. A) Heatmap of sEV-lncRNA differential expression analysis between BM–infiltrated (red rectangles) and non-infiltrated (blue rectangles) patients. Each column represents a patient, and each row corresponds to a specific lncRNA. Expression values are reported as Z-scores and visualized using a color scale, with blue indicating downregulation and red indicating upregulation relative to the mean. B) Enriched biological pathways targeted by lncRNAs. The graph reports the main cellular biological categories resulted from miRNet analysis.

5.3.2 Integrating the expression of BM-derived sEV genes, miRNA and lncRNA improves HR-NB patient stratification.

To assess whether the comprehensive gene and small RNA profiling of BM-sEVs could improve the stratification of HR-NB with and without BM infiltration characterized by poor prognosis, we integrated the data with Movics, a data integration R package (see Material and Methods). The results of the analysis were reported in the heatmap of Figure 14 A. The unsupervised hierarchical clustering based on integrated RNA expression of BM-sEVs led to the identification of three different clusters (CS1-3). Cluster CS3 included patients with an sEV-RNA profile associated with the highest degree of BM infiltration, while CS2 showed the enrichment of samples with high levels of expression (over the median) of the hypoxia signature, related to unfavorable outcome[41]. The association with the tumor hypoxic status was performed by comparing sEV-RNA sequencing results with the publicly available dataset published by Cangelosi et al.[41], who clearly demonstrated the existence of a hypoxic signature at gene expression level in NB primary tumors, which was strongly associated with a poor clinical outcome. We performed the integrate pathway analysis of the ten genes, miRNAs and lncRNAs, reported in Figure 14 B, that contributed the most in cluster identification. Results showed that the enriched biological pathways belong to immune response regulation, signaling pathways, especially PI3K/Akt and Wnt/β catenin pathways, cytoskeleton dynamics, apoptosis, cell metabolism and developmental processes. These results confirmed that EV-RNAs modulated in HR-NB patients with BM infiltration are involved in immune response, potentially shaping an immunosuppressive TME. These findings suggested that the integration of sEV-RNA profiling could identify subsets of patients not only associated to BM infiltration, but also potentially associated to the clinical outcome: CS2 included patients strongly associated with hypoxic tumor status, thus characterized by a poor clinical outcome. Unfortunately, due to the need of a 5-year follow up and to the low number of patients included in the clusters identified, we could not perform a significant association with the overall survival at this stage. Therefore, to define the prognostic value of the identified circulating markers we will extend HR-NB patient cohort.

However, before evaluating the association of sEV-RNA markers with patient clinical outcome, it is mandatory to validate the biological relevance of RNA sequencing data with a more sensitive technique.

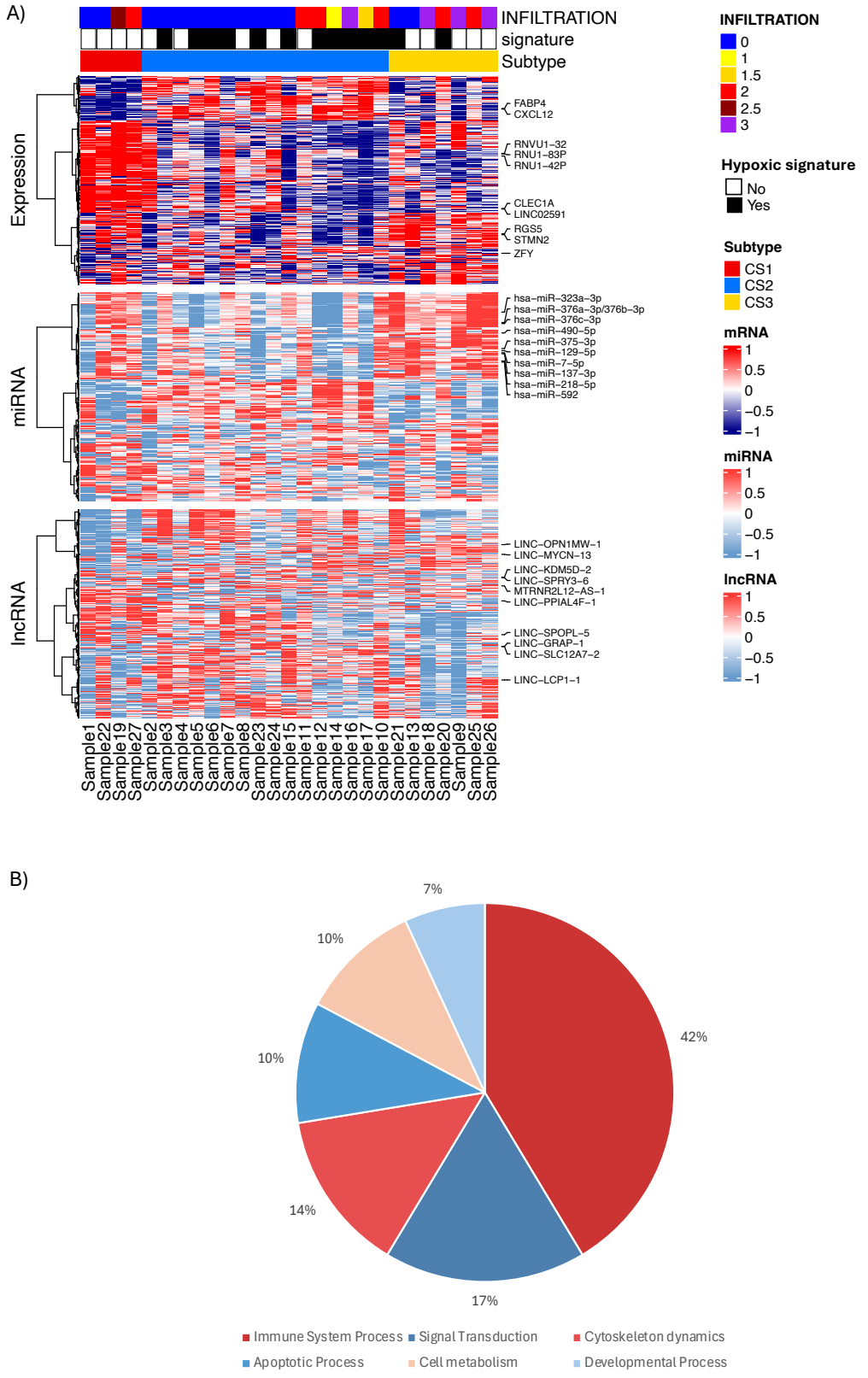

Figure 14: Integrative sEV-RNA analysis. A) Heatmap of integrated differential expression analysis of sEV-RNAs. Each column represents a patient, and each row corresponds to a specific sEV-mRNA, -miRNA and -lncRNA. Expression values are reported as Z-scores and visualized using a color scale, with blue indicating downregulation and red indicating upregulation relative to the mean. B) Enriched biological pathways targeted by the most significant sEV-RNAs contributing to the identification of clusters CS1-3 reported on the heatmap. The graph reports the main cellular biological categories resulted from miRNet analysis.

5.4 EV-miRNA expression validation through a digital PCR assay

To identify the most relevant sEV-miRNA able to discriminate between NB patients with and without BM infiltration we performed receiver operating characteristic (ROC) analysis. ROC results may assist in narrowing down the number of miRNAs, thereby facilitating the identification of promising targets to be validated.

ROC curve graphically represents sensitivity, rate of true positives, versus 1-specificity, which indicates the rate of false positives. The area under the curve (AUC) determines discriminating variable ability: the closer the AUC value is to 1, the higher the power of the variable to discriminate between the two groups considered. When the AUC value is equal to or lower than 0.5, the variable has no discriminant ability. ROC analysis was performed with MedCalc Software at its latest version. Statistical significance of the AUC was assessed using the z-test, with standard error estimated according to the method of DeLong's test.

ROC analysis results are reported in Figure 15. Among the 15 sEV-miRNAs significantly differentially expressed, miR-652-3p, miR-23a-3p, miR-200c-3p, miR-21-5p, and miR-576-5p showed good AUC values ranging from 0.819 to 0.890, with p-values < 0.001. The combination of high AUC values and strong statistical significance indicates that these miRNAs can discriminate between BM infiltrated and BM non-infiltrated samples.

Experimentally validated miRNA targets were identified through a literature review. miR-23a negatively regulates autophagy-related protein 12 (ATG12), thereby suppressing the autophagy process. In metastatic melanoma, miR-23a is significantly downregulated, resulting in increased ATG12 expression, enhanced autophagy, and promotion of metastatic behavior[42]. miR-652-3p targets paired related homeobox 1 (PRRX1), also known as PHOX1: downregulation of miR-652-3p may contribute to tumor progression in GH-producing pituitary tumors[43].

Interestingly, miR-576-5p, miR-200c-3p, and miR-21-5p are directly or indirectly involved in the regulation of PD-L1 expression. miR-576-5p targets oncogenic signaling pathways regulating PD-L1 expression, including PI3K/AKT/mTOR, and Wnt/β-catenin[44,45]. In ovarian cancer it has been reported that miR-200c can directly inhibit PD-L1 expression and reduce cancer cell proliferation through the downregulation of c-Myc and β-catenin, resulting in increased sensitivity towards therapeutic treatment[46]. Finally, it has been shown thatmiR-21 inhibition improves sensitivity of PD-L1 expressing tumors to PD1/PD-L1 blockade, affecting PD-L1-associated immune evasion[47].

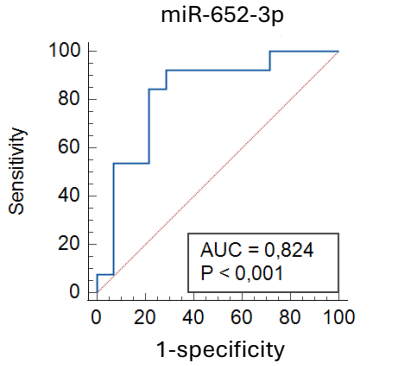

Sensitivity (%)	Specificity (%)
92.3	71.4

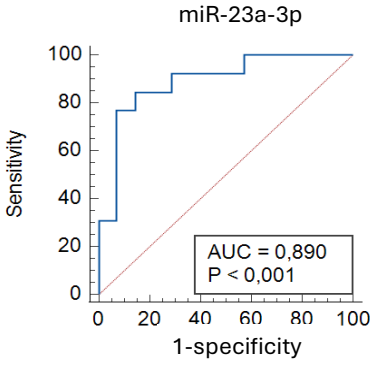

Sensitivity (%)	Specificity (%)
84.6	85.7

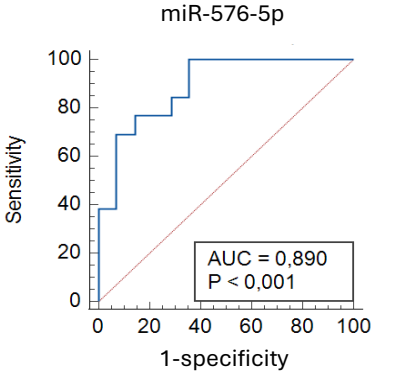

Sensitivity (%)	Specificity (%)
100	64.3

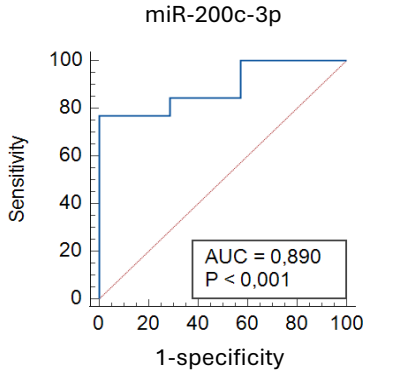

Sensitivity (%)	Specificity (%)
76.9	100

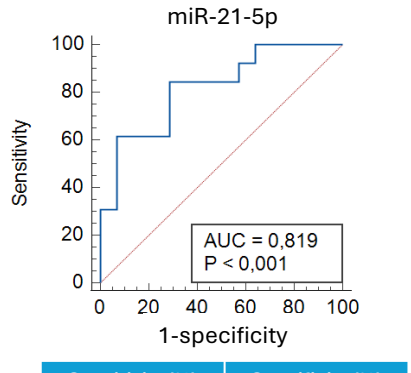

Sensitivity (%)	Specificity (%)
84.6	71.4

Figure 15: Discriminant ability of miRNA-652-3p, miRNA-23a-3p, miR-576-5p, miR-200c-3p and miR-21-5p. ROC curves display the false positive rate (1 – specificity) on the X-axis and the true positive rate (sensitivity) on the Y-axis. The red diagonal line indicates an AUC of 0.5, representing no discriminative ability. For each miRNA, the area under the curve (AUC) and p-value are reported. Tables below the ROC graphs summarize the sensitivity and specificity of each miRNA.

Considering their biological role, and the highest AUC values reported by ROC analysis, we focused on miR-200c-3p and miR-576-5p to set up the validation protocol based on dPCR. Indeed, the lack of a standard reference in sEV-miRNA expression analysis hinders the use of RTqPCR for validation, thus dPCR represents a more reliable method, as it enables the absolute quantification without the need for a standard curve or references.

We implemented a dPCR validation protocol specific for sEV-miRNA evaluation by assessing sEV-miR-200c-3p and miR-576-5p in a subset of our cohort of patients, including HR-NB patients with (n=6) and without (n=5) BM infiltration. An example of dPCR results visualized with 1D scatter plot is reported in Figure 16 A: each blue dot in the graph represents the fluorescence intensity measured for a single PCR reaction occurring in a single well. Grey dots indicate wells where no cDNA fragments were detected (negative signal), while the red line marks the positivity threshold.

The absolute quantification values are expressed as copies per microliter (cp/µL), as reported in Figure 16 A.

The results of this preliminary validation confirmed the significant ($p<0.05$) downregulation of sEV-miR-200c in NB patients with BM infiltration (Figure 16 B, left panel). Although we also observed the downregulation of sEV-miR-576-5p in BM-infiltrated samples (Figure 16 B, right panel), the differential expression was not significant.

Overall, these findings showed the efficient implementation of a dPCR-based protocol for the validation of RNAseq data, confirming the significant reduction in sEV-miR-200c-3p levels in BM samples with NB cell infiltration. Extending the validation cohort might confirm a significant downregulation of miR-576-5p. The implemented dPCR protocol will be employed to assess the sEV-miRNA biomarkers identified, aiming at validating these data in an independent cohort of patients to establish their prognostic value.

A)

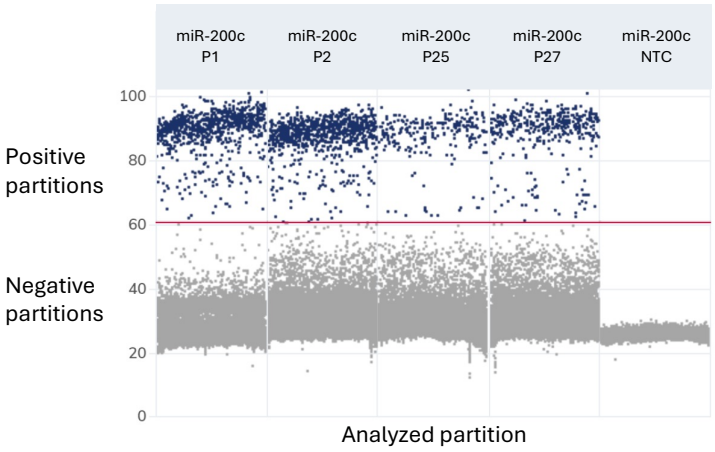

	P1 BM neg	P2 BM neg	P25 BM pos	P27 BM pos
Conc (cp/µL)	45.24	51.82	13.22	21.52
CI (95%)	6.9%	6.4 %	12.8%	10%

B)

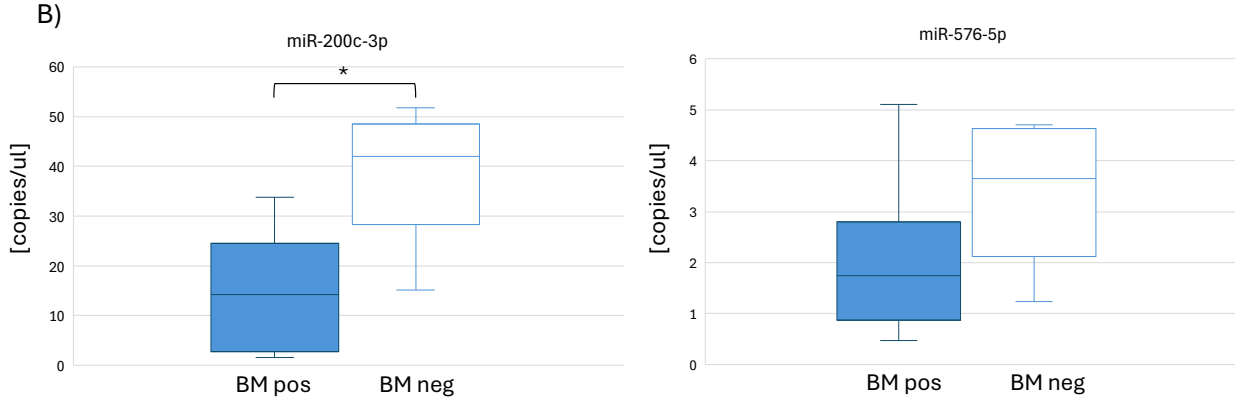

Figure 16: sEV-miRNA expression differences measured by digital PCR. (A) The 1D scatter plots, from left to right, show sEV-miR-200c expression of BM non-infiltrated (BM neg) patients (P1 and P2), BM-infiltrated (BM pos) patients (P25 and P27), and the negative control (NTC). Positive and negative partitions, expressed in relative fluorescence units (RFU), are reported on the Y-axis. The red line indicates the positivity threshold that separates positive signals (blue dots) from negative signals (grey dots). The table reports miRNA quantification expressed in cp/µl and and 95% confidence interval. Conc = concentration. (B) Boxplots showing miR-200c-3p and miR-576-5p expression measured by dPCR in the validation subsets of BM pos (n=6) and BM neg (n=5) patients. The absolute quantification, expressed as copies/µl is reported on the Y axis. P value resulting from T-test analysis is reported.

6. Discussion

Liquid biopsy studies in pediatric oncology have increased in the past decade, as they represent an important source of biomarkers with diagnostic and prognostic value. Liquid biopsies have been largely investigated in NB, especially in terms of circulating tumor DNA, circulating RNAs and EVs. Such studies focused mainly on PB as a non-invasive source of biomarkers, allowing the longitudinal monitoring of the disease. However, BM represent the main metastatic niche for HR-NB patients and it is characterized by the presence of an immunosuppressive TME that hinders and limits the efficacy of the current standard treatment including immunotherapy. To explain the immunosuppressive features of the TME, several studies aimed at characterizing the cellular composition of the BM. However, BM-derived EVs, which play a key role in the crosstalk between tumor cells and TME components, are still poorly investigated. A recent study characterized proteins expressed on EV surface[31], but information on BM-derived EV-RNA content is still lacking.

With the present study we aimed at assessing potential differences in the sEV-RNA expression profile between HR-NB patients with and without BM infiltration. The results may help in understanding mechanisms contributing to the immunosuppressive BM TME responsible for immunotherapy resistance and identifying novel biomarkers potentially improving current standard treatments.

Our results showed the efficacy of a SEC-based method for the efficient isolation of sEVs from a complex biological fluid as BM. We observed that sEVs isolated from PB and BM showed comparable quantitative and qualitative data. Notably, sEVs isolated from PB displayed a size distribution consistent with findings reported in previous studies[24]. Given that PB has been more extensively investigated[24] and it is easier to process than BM due to its lower biological complexity, these findings support the efficiency of the implemented protocol for sEV isolation from BM, enabling to collect significant amounts of vesicles. The efficiency of the implemented method was further supported by the homogeneity of the vesicles obtained, as confirmed by the low PDI recorded. The vesicle size was analyzed with three different techniques, confirming a diameter ranging between 100 nm and 160 nm.

sEVs morphological evaluation by TEM revealed a round shape with a high density of content. sEVs at TEM analysis are usually characterized by evident membrane and cut-shape morphology, which aren't visible in this analysis: several data have been published on EVs derived from NB cell lines[48] but not on EVs isolated directly from patient samples, especially from BM, thus, few data are available to compare results. However, TEM analysis detected the presence of integer sEVs.

While mRNA analysis did not highlight significant differences between HR-NB patients with and without BM infiltration, small RNA showed a significant differential expression profile in terms of

sEV-miRNAs and sEV-lncRNAs in BM infiltrated samples compared to non-infiltrated ones, thus indicating the huge presence of post-transcriptional regulatory mechanisms.

We specifically observed the significant downregulation of 15 miRNAs in BM-infiltrated patients. Pathway analysis revealed that these sEV-miRNA were involved in biological processes associated with tumor progression and aggressiveness, such as PI3K-Akt signaling, p53 signaling, NF-kappa B signaling, VEGF signaling, and ECM-receptor interaction.

In NB, the pro-survival phosphatidylinositol 3-kinase (PI3K)/protein kinase B (also known as PKB or AKT) pathway is often overactivated[49]. Among the three isoforms of the AKT/PKB family of kinases, AKT1 is the most frequently altered in multiple tumor types and is involved in promoting tumor cell growth and migration[50]. p53 and NF-Kappa B are nuclear transcription factors that play important and opposite roles in cell survival: the former is one of the most well-known tumor suppressor gene, inducing apoptosis by inhibiting Bcl-2 protein and activating the pro-apoptotic protein BAX. In NB, p53 is rarely mutated in NB at diagnosis but the mutation frequency increases at relapse and is associated with poor prognosis[51].

sEVs derived from infiltrated BM samples showed also a distinct lncRNA expression profile compared to non-infiltrated ones. Interestingly, similarly to sEV-miRNAs, modulated lncRNAs were mainly involved in the immune system response, in cell signaling and apoptotic process. These findings pointed out that sEVs derived from infiltrated BM samples showed a specific RNA expression profile consistent with immune-related functions and potentially involved in the regulation of immune processes, thus this can actively contribute to the establishment of the immunosuppressive TME observed in the BM metastatic niche.

It is known that the BM metastatic niche shows a heterogeneous cellular composition, but the limited volume availability of pediatric specimens did not allow us to determine the cellular origin of isolated sEVs which, thus, can be released by both tumor and non-tumor cell populations.

Integrative analysis of sEV-mRNA, -miRNA and -lncRNA identified three different clusters of HR-NB patients, highlighting that the CS2 cluster was significantly associated with hypoxia, indicative of poor prognosis in HR-NB patients[41]. Indeed, CS2 has been correlated with the hypoxia signature identified by Cangelosi et al.[41], who reported a specific hypoxia-related transcription profile that represents an independent risk factor for NB, identifying patients with poor clinical outcome. According to our data, we hypothesize that cluster CS2 may include patients with a more aggressive disease, who can be identified through the hypoxic tumor status and the integrated sEV-RNA expression profile. However, at this stage, the limited sample size and the lack of a 5-year follow-up hindered the correlation analysis with clinical outcome, thereby limiting further investigation of this hypothesis. Interestingly, among the genes mainly contributing to the stratification in three different

clusters of patients we detected CXCL12 and FABP4. We observed a high expression of CXCL12 in sEVs derived from patients belonging to CS2, which was associated to poor prognosis. However, it has previously been reported that tumor NB cells in the BM do not express high levels CXCL12[52]. Therefore, while we could not directly demonstrate the cellular origin of CXCL12 expressing sEVs, these findings support the hypothesis that CXCL12-enriched sEVs originate mainly from the BM microenvironment, including stromal, mesenchymal or myeloid cell populations which might selectively upregulate CXCL12 and load its transcript inside EVs. The enrichment of CXCL12 positive sEVs in the cluster of patients characterized by poor prognosis suggests that the activation of CXCL12 axis in the BM niche contribute to the establishment of a TME supporting NB cell growth, dissemination and retention. In line with this hypothesis, it has been demonstrated that NB cells exposed to conditioned media mimicking BM niche increased the expression of CXCR4, which is a receptor for CXCL12[53]. The activated CXCL12/CXCR4 axis promoted NB cell proliferation, migration and invasion, thus supporting an aggressive tumor phenotype.

FABP4 protein expression on tumor associated macrophages exert pro-tumoral effect in NB[54]. Indeed, it has been shown that FABP4-mediated macrophages promote NB tumor cell proliferation and migration both *in vivo* and *in vitro*, and it has been associated to poor clinical outcome. FABP4 inactivates NF-κB/RelA-IL1α pathway, maintaining macrophages into an anti-inflammatory M2 phenotype, and, thus, limiting the efficacy of immunotherapy.

Although the association between clinical outcome and HR-NB patient clusters identified by differentially expressed sEV-RNA must be assessed in an independent and broader study cohort, it is also mandatory to experimentally validate the differential expression identified by RNA sequencing. Considering the potential value of differentially expressed sEV-RNAs in discriminating between infiltrated and non-infiltrated BM samples and in stratifying HR-NB patients, we aimed at validating the results by implementing a digital PCR-based assay. The assay was implemented starting from sEV-miRNAs. To this end, we first selected the sEV-miRNA that could significantly discriminate between patients with and without BM infiltration. To this end, ROC analysis identified five miRNAs with great sensitivity and specificity values in discriminating the two groups considered: miR-652-3p, miR-23a-3p, miR-200c-3p, miR-21-5p, and miR-576-5p. Among them we focused specifically on miR-576-5p, miR-200c-3p, and miR-21-5p because of their direct and indirect regulation of PD-L1 expression. Specifically, PD-L1 direct targeting is exerted by miR-200c, consistent with the hypothesis of PD-L1 increased expression in NB patients with BM infiltration. In contrast, miR-576-5p and miR-21 have been involved in PD-L1 regulation through indirect mechanisms, acting on upstream biological pathways[44-46]. Based on both biological rationale and ROC analysis results, we prioritized the validation of miR-200c-3p and miR-576-5p, facilitating the implementation of a

rigorous validation protocol. The dPCR analysis on a subset of HR-NB patients confirmed the downregulation of both miR-200c-3p and miR-576-5p in NB-infiltrating samples, although statistical significance was reported only for miR-200c-3p. These findings pointed out miR-200c as a strong candidate biomarker for monitoring BM infiltration and potentially identifying patients with increased PD-L1 expression.

The PD-1/PD-L1 pathway is a key immune checkpoint that promotes immune evasion by inhibiting T and NK cell activation. The sEV-miRNA content might reflect increased PD-L1 expression on neoplastic and non-neoplastic cells within the TME, supporting the role of this biological axis in establishing an immunosuppressive phenotype. While tumor cells represent a major source of immunosuppressive signals, PD-L1 has also been reported on immune cell subsets including T, NK cells, macrophages and dendritic cells which establish functional cross-talks. In this context, PD-L1 expression has been associated with the presence of a pro-inflammatory milieu, making patients more sensitive to therapies based on PD1/PD-L1 blockade[55]. We hypothesize that sEVs containing low levels of miR-200c-3p, miR-576-5p and miR-21-5p might reflect the upregulation of PD-L1 expression in the origin releasing cells. Such correlation as possible immunological consequence of the observed sEV-miRNA modulation is reported in Figure 18.

To address this point, additional flow-cytometry studies are needed (i) to evaluate PD-L1 expression on specific cell subsets, and (ii) to determine the origin of sEVs to better understand which cellular subsets mainly regulate the TME within the metastatic BM niche. In addition, the potential immunosuppressive effects of sEVs could be explored by analyzing immune cell activation and function in co-culture experiments with T and NK cells.

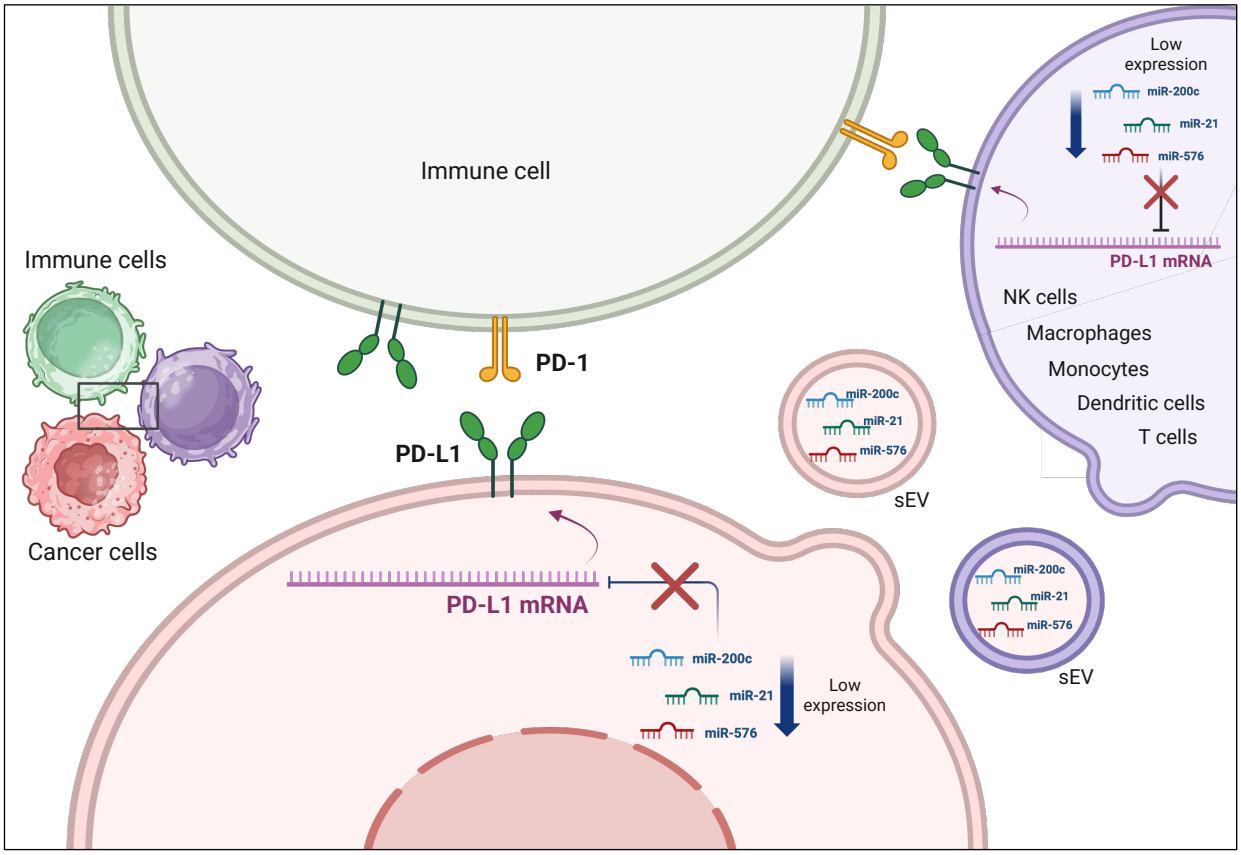

Figure 18: The image illustrates the potential impact of miR-576-5p, miR-200c-3p, and miR-21-5p on PD-L1 expression, highlighting the inverse correlation between their downregulation in sEVs and the upregulation of PD-L1 on sEVs or the cell surface [created with BioRender.com].

The present study provided useful insight into the role of sEVs within the BM of NB patients. Validation of established immune checkpoints in novel contexts, such as infiltrated BM in NB patients, could refine immunotherapy strategies by identifying more targeted and condition-specific approaches to reduce the risk of relapse in HR-NB patients.

Although the data on sEV-RNA profiling must be validated in an independent and broader cohort of patients with a 5 year follow up, these results provided the first insights of the key role of sEVs in modulating the immune response within the BM metastatic niche.

Nucleic acid-based therapies targeting the identified miRNA and lncRNA could be explored for their potential combination with current treatment[56,57]. As previously mentioned, it has been demonstrated that targeting the PD-1/PD-L1 axis can improve HR-NB patient response to immunotherapy with anti-GD2 antibody[58,59]. Blocking such axis in immune cells leads to the increase of INF-γ, which triggers PD-L1 expression, making tumor cells more sensitive to immunotherapies based on PD1/PD-L1 blockade.

Targeting sEV-RNA involved in this axis as the ones we identified with novel nucleic acid-based therapeutics might help in increasing the response of HR-NB patients to immunotherapy, reducing

the risk of fatal relapse. Moreover, the sensitive dPCR assay we implemented specifically for such markers could be easily translated to a clinical setting to assess the eligibility of HR-NB patients to such combination therapy.

7. Conclusions

The present study represents the first characterization of BM-derived sEV-RNA profiling in HR-NB patients, pointing out their role in shaping the immunosuppressive TME observed in the BM metastatic niche. We identified sEV-miRNA and -lncRNAs differentially expressed between infiltrated and non-infiltrated BM samples and data integration of all sEV RNA species stratified HR-NB patient into clinically relevant subsets. These findings provide the first evidence of the biological function of BM-sEVs as active mediators of TME interactions, regulating immune regulation, cell signaling and metabolism. Moreover, the implementation of a sensitive dPCR-based assay to measure selected sEV-RNAs supports the translational applicability of our results, paving the way for the development of a fast and reliable evaluation of markers to adopt personalized therapeutic solutions. Although validation in larger cohorts is mandatory, our data highlight BM-derived sEVs as promising candidates for both mechanistic studies and therapeutic investigation, offering novel approaches to enhance immunotherapy efficacy and reducing the risk of relapse in HR-NB patients.

8. References

1. Campbell K, Siegel DA, Umaretiya PJ, et al. A comprehensive analysis of neuroblastoma incidence, survival, and racial and ethnic disparities from 2001 to 2019. *Pediatr Blood Cancer*. 2024;71(1):e30732. doi: 10.1002/pbc.30732.
2. Rainusso N, Seghers V, Egler R, et al. Neuroblastoma of the Bone and Bone Marrow Without an Apparent Primary Site: Report of 4 Cases With Long-term Follow-up. Pediatric and *Developmental Pathology*. 2019; 22(4):329-333. doi:10.1177/1093526618822597
3. Tolbert VP, Matthay KK. Neuroblastoma: clinical and biological approach to risk stratification and treatment. *Cell Tissue Res*. 2018; 372(2):195-209. doi: 10.1007/s00441-018-2821-2.
4. Soldatov R, Kaucka M, Kastriti M.E, et al. Spatiotemporal structure of cell fate decisions in murine neural crest. *Science*. 2019; 364(6444): eaas9536. doi: 10.1126/science.aas9536.
5. Ponzoni M, Bachetti T, Corrias MV, et al. Recent advances in the developmental origin of neuroblastoma: an overview. *J Exp Clin Cancer Res*. 2022; 41(1):92. doi: 10.1186/s13046-022-02281-w.
6. Simões-Costa M, Bronner ME. Establishing neural crest identity: a gene regulatory recipe. *Development*. 2015;142(2):242-57. doi: 10.1242/dev.105445
7. Higashi M, Sakai K, Fumino S, et al. The roles played by the MYCN, Trk, and ALK genes in neuroblastoma and neural development. *Surg Today*. 2019; 49(9):721-727. doi: 10.1007/s00595-019-01790-0
8. Brodeur GM, Pritchard J, Berthold F, et al. Revisions of the international criteria for neuroblastoma diagnosis, staging, and response to treatment. *J Clin Oncol*. 1993;11(8):1466-77. doi: 10.1200/JCO.1993.11.8.1466
9. Monclair T, Brodeur GM, Ambros PF, et al. The International Neuroblastoma Risk Group (INRG) staging system: an INRG Task Force report. *J Clin Oncol*. 2009; 27(2):298-303. doi: 10.1200/JCO.2008.16.6876.
10. Sokol E, Desai AV. The Evolution of Risk Classification for Neuroblastoma. *Children (Basel)*. 2019; 6(2):27. doi: 10.3390/children6020027.
11. Liang WH, Federico SM, London WB, et al. Tailoring Therapy for Children With Neuroblastoma on the Basis of Risk Group Classification: Past, Present, and Future. *JCO Clin Cancer Inform*. 2020; 4:895-905. doi: 10.1200/CCI.20.00074.
12. Imamura T, Komatsu S, Ichikawa D, et al. Liquid biopsy in patients with pancreatic cancer: Circulating tumor cells and cell-free nucleic acids. *World J Gastroenterol*. 2016; 22(25):5627-41. doi: 10.3748/wjg.v22.i25.5627.
13. Tan HN, Elliott MJ, Silverman IM, et al. Circulating tumor DNA as a biomarker in early phase clinical trials. *Cancer Cell*. 2025; S1535-6108(25)00504-5. doi: 10.1016/j.ccell.2025.11.011.
14. Pierri B, Eitan E, Witwer KW, et al. Tissue-Specific Extracellular Vesicles Enriched From Circulation: Exploring the Liquid Biopsy Perspective. J Extracell Biol. 202; 5(2):e70106. doi: 10.1002/jex2.70106
15. Fernández-Lázaro D, Hernández JLG, García AC, et al. Clinical Perspective and Translational Oncology of Liquid Biopsy. *Diagnostics (Basel)*. 2020; 10(7):443. doi: 10.3390/diagnostics10070443.
16. Van Zogchel LMJ, Decarolis B, Van Wezel EM, et al. Sensitive liquid biopsy monitoring correlates with outcome in the prospective international GPOH-DCOG high-risk neuroblastoma RT-qPCR validation study. *J Exp Clin Cancer Res*. 2024; 43(1):331. doi: 10.1186/s13046-024-03261-y.
17. Johnson KB, Wei WQ, Weeraratne D, et al. Precision Medicine, AI, and the Future of Personalized Health Care. *Clin Transl Sci*. 2021;14(1):86-93. doi: 10.1111/cts.12884.
18. Gurung, S, Perocheau D, Touramanidou L, Baruteau, J. The exosome journey: from biogenesis to uptake and intracellular signalling. Cell Commun Signal. 2021; 19(1):47. doi: 10.1186/s12964-021-00730-1.

19. Beck S, Hochreiter B, Schmid JA. Extracellular Vesicles Linking Inflammation, Cancer and Thrombotic Risks. *Front Cell Dev Biol*. 2022; 10:859863. doi: 10.3389/fcell.2022.859863.
20. Zakirova EY, Aimaletdinov AM, Malanyeva AG, et al. Extracellular Vesicles: New Perspectives of Regenerative and Reproductive Veterinary Medicine. *Front Vet Sci*. 2020; 7:594044. doi: 10.3389/fvets.2020.594044.
21. Liu YJ, Wang C. A review of the regulatory mechanisms of extracellular vesicles-mediated intercellular communication. *Cell Commun Signal*. 2023; 21(1):77. doi: 10.1186/s12964-023-01103-6.
22. Mohamed AH, Abaza T, Youssef YA, et al. Extracellular vesicles: from intracellular trafficking molecules to fully fortified delivery vehicles for cancer therapeutics. *Nanoscale Adv*. 2025; 7(4):934-962. doi: 10.1039/d4na00393d.
23. Qin Z, Xu Q, Hu H, et al. Extracellular Vesicles in Renal Cell Carcinoma: Multifaceted Roles and Potential Applications Identified by Experimental and Computational Methods. *Front Oncol*. 2020;10:724. doi: 10.3389/fonc.2020.00724.
24. Morini M, Cangelosi D, Segalerba D, et al. Exosomal microRNAs from Longitudinal Liquid Biopsies for the Prediction of Response to Induction Chemotherapy in High-Risk Neuroblastoma Patients: A Proof of Concept SIOPEN Study. *Cancers (Basel)*. 2019; 11(10):1476. doi: 10.3390/cancers11101476.
25. Morini M, Raggi F, Bartolucci M, et al. Plasma-Derived Exosome Proteins as Novel Diagnostic and Prognostic Biomarkers in Neuroblastoma Patients. *Cells*. 2023; 12(21):2516. doi: 10.3390/cells12212516.
26. Hanahan D, Weinberg RA. Hallmarks of cancer: the next generation. *Cell*. 2011; 144(5):646-74. doi: 10.1016/j.cell.2011.02.013.
27. Brignole C, Pastorino F, Perri P, et al. Bone Marrow Environment in Metastatic Neuroblastoma. *Cancers (Basel)*. 2021;13(10):2467. doi: 10.3390/cancers13102467.
28. Burchill SA, Beiske K, Shimada H, et al. Recommendations for the standardization of bone marrow disease assessment and reporting in children with neuroblastoma on behalf of the International Neuroblastoma Response Criteria Bone Marrow Working Group. *Cancer*. 2017; 123(7):1095-1105. doi: 10.1002/cncr.30380.
29. Mei S, Alchahin AM, Embaie BT, et al. Single-cell analyses of metastatic bone marrow in human neuroblastoma reveals microenvironmental remodeling and metastatic signature. *JCI Insight*. 2024; 9(6):e173337. doi: 10.1172/jci.insight.173337.
30. Hochheuser C, Van Zogchel LMJ, Kleijer M, et al. The Metastatic Bone Marrow Niche in Neuroblastoma: Altered Phenotype and Function of Mesenchymal Stromal Cells. *Cancers (Basel)*. 2020;12(11):3231. doi: 10.3390/cancers12113231
31. Marimpietri D, Corrias MV, Tripodi G, et al. Immunomodulatory properties of extracellular vesicles isolated from bone marrow of patients with neuroblastoma: role of PD-L1 and HLA-*G*. *Front Immunol*. 2024;15:1469771. doi: 10.3389/fimmu.2024.1469771.
32. Morini M, Vitale C, Ardito M, et al. Exosomes and immune modulation: implications for neuroblastoma immunotherapy. *Front Immunol*. 2025; 16:1600062. doi: 10.3389/fimmu.2025.1600062.
33. Patil AH, Halushka MK. miRge3.0: a comprehensive microRNA and tRF sequencing analysis pipeline. *NAR Genom Bioinform*. 2021; 3(3):lqab068. doi: 10.1093/nargab/lqab068
34. Tusher VG, Tibshirani R, Chu G. Significance analysis of microarrays applied to the ionizing radiation response. *Proc Natl Acad Sci USA*. 2001; 98(9): 5116-21. doi: 10.1073/pnas.091062498.
35. Lu X, Meng J, Zhou Y, et al. MOVICS: an R package for multi-omics integration and visualization in cancer subtyping. *Bioinformatics*. 2021; 36(22-23):5539-5541. doi: 10.1093/bioinformatics/btaa1018.
36. Love MI, Huber W, Anders S. Moderated estimation of fold change and dispersion for RNA-seq data with DESeq2. *Genome Biol*. 2014;15(12):550. doi: 10.1186/s13059-014-0550-8.
37. DeLong ER, DeLong DM, Clarke-Pearson DL. Comparing the areas under two or more correlated receiver operating characteristic curves: a nonparametric approach. *Biometrics*. 1988;44(3):837-45.

38. Colonna M. DAP12 signaling: from immune cells to bone modeling and brain myelination. *J Clin Invest*. 2003; 111(3):313-4. doi: 10.1172/JCI17745.
39. Duan X, Wu R, Zhang M, et al. The heterogeneity of NOTCH1 to tumor immune infiltration in pan-cancer. *Sci Rep*. 2024; 14(1):28071. doi: 10.1038/s41598-024-79883-1. Erratum in: Sci Rep. 2025 Feb 5;15(1):4382. doi: 10.1038/s41598-025-87306-y.
40. He Y, Sun MM, Zhang GG, et al. Targeting PI3K/Akt signal transduction for cancer therapy. Signal Transduct Target Ther. 2021; 6(1):425. doi: 10.1038/s41392-021-00828-5
41. Cangelosi D, Morini M, Zanardi N, et al. Hypoxia Predicts Poor Prognosis in Neuroblastoma Patients and Associates with Biological Mechanisms Involved in Telomerase Activation and Tumor Microenvironment Reprogramming. *Cancers (Basel)*. 2020; 12(9):2343. doi: 10.3390/cancers12092343
42. Guo W, Wang H, Yang Y, et al. Down-regulated miR-23a Contributes to the Metastasis of Cutaneous Melanoma by Promoting Autophagy. *Theranostics*. 2017; 7(8):2231-2249. doi: 10.7150/thno.18835
43. Lee YJ, Kang CW, Oh JH, et al. Downregulation of miR-216a-5p and miR-652-3p is associated with growth and invasion by targeting JAK2 and PRRX1 in GH-producing pituitary tumours. *J Mol Endocrinol*. 2021; 68(1):51-62. doi: 10.1530/JME-21-0070.
44. Hadavi R, Mohammadi-Yeganeh S, Razaviyan J, et al. Expression of Bioinformatically Candidate miRNAs including, miR-576-5p, miR-501-3p and miR-3143, Targeting PI3K Pathway in Triple-Negative Breast Cancer. *Galen Med J*. 2019; 8:e1646. doi: 10.31661/gmj.v8i0.1646.
45. Luo J, Liu L, Shen J, Zhou N, Feng Y, Zhang N, Sun Q, Zhu Y. miR-576-5p promotes epithelial-to-mesenchymal transition in colorectal cancer by targeting the Wnt5a-mediated Wnt/β-catenin signaling pathway. *Mol Med Rep*. 2021; 23(2):94. doi: 10.3892/mmr.2020.11733.
46. Anastasiadou E, Messina E, Sanavia T, et al. MiR-200c-3p Contrasts PD-L1 Induction by Combinatorial Therapies and Slows Proliferation of Epithelial Ovarian Cancer through Downregulation of β-Catenin and c-Myc. *Cells*. 2021; 10(3):519. doi: 10.3390/cells10030519.
47. Kim EH, Choi J, Jang H, et al. Targeted delivery of anti-miRNA21 sensitizes PD-L1^{high} tumor to immunotherapy by promoting immunogenic cell death. *Theranostics*. 2024;14(10):3777-3792. doi: 10.7150/thno.97755.
48. Haug BH, Hald ØH, Utnes P, et al. Exosome-like Extracellular Vesicles from MYCN-amplified Neuroblastoma Cells Contain Oncogenic miRNAs. *Anticancer Res*. 2015; 35(5):2521-30
49. Zafar A, Wang W, Liu G, et al. Molecular targeting therapies for neuroblastoma: Progress and challenges. *Med Res Rev*. 2021; 41(2):961-1021. doi: 10.1002/med.21750. Erratum in: Med Res Rev. 2022 Jan;42(1):641. doi: 10.1002/med.21843
50. Khezri MR, Jafari R, Yousefi K. The PI3K/AKT signaling pathway in cancer: Molecular mechanisms and possible therapeutic interventions. *Exp Mol Pathol*. 2022; 127:104787. doi: 10.1016/j.yexmp.2022.104787
51. Almeida J, Mota I, Skoda J, Sousa E, Cidade H, Saraiva L. Deciphering the Role of p53 and TAp73 in Neuroblastoma: From Pathogenesis to Treatment. *Cancers (Basel)*. 2022; 14(24):6212. doi: 10.3390/cancers14246212.
52. Scaruffi P, Morandi F, Gallo F, et al. Bone marrow of neuroblastoma patients shows downregulation of CXCL12 expression and presence of IFN signature. *Pediatr Blood Cancer*. 2012; 59(1):44-51. doi: 10.1002/pbc.23339.
53. Garcia-Gerique L, García M, Garrido-Garcia A, et al. MIF/CXCR4 signaling axis contributes to survival, invasion, and drug resistance of metastatic neuroblastoma cells in the bone marrow microenvironment. *BMC Cancer*. 2022; 22(1):669. doi: 10.1186/s12885-022-09725-8.
54. Miao L, Zhuo Z, Tang J, et al. FABP4 deactivates NF-κB-IL1α pathway by ubiquitinating ATPB in tumor-associated macrophages and promotes neuroblastoma progression. *Clin Transl Med*. 2021; 11(4):e395. doi: 10.1002/ctm2.395
55. Tang F, Zheng P. Tumor cells versus host immune cells: whose PD-L1 contributes to PD-1/PD-L1 blockade mediated cancer immunotherapy? *Cell Biosci*. 2018; 8:34. doi: 10.1186/s13578-018-0232-4.

56. Christopher AF, Kaur RP, Kaur G, et al. MicroRNA therapeutics: Discovering novel targets and developing specific therapy. *Perspect Clin Res*. 2016; 7(2):68-74. doi: 10.4103/2229-3485.179431.
57. Arun G, Diermeier SD, Spector DL. Therapeutic Targeting of Long Non-Coding RNAs in Cancer. *Trends Mol Med*. 2018; 24(3):257-277. doi: 10.1016/j.molmed.2018.01.001
58. Siebert N, Zumpe M, Jüttner M, et al. PD-1 blockade augments anti-neuroblastoma immune response induced by anti-GD2 antibody ch14.18/CHO. *Oncoimmunology*. 2017; 6(10):e1343775. doi: 10.1080/2162402X.2017.1343775.
59. Dondero A, Pastorino F, Della Chiesa M, et al. PD-L1 expression in metastatic neuroblastoma as an additional mechanism for limiting immune surveillance. *Oncoimmunology*. 2015; 5(1):e1064578. doi: 10.1080/2162402X.2015.1064578.